PL-TR-95-2103

ANALYZE DATA FROM CRRES PAYLOADS AFGL-701-2/DOSIMETER AND AFGL-701-4/HEEF

Frederick A. Hanser

PANAMETRICS, INC.
221 Crescent Street
Waltham, MA 02154-3497

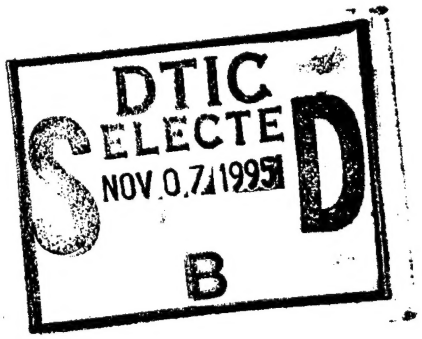

26 July 1995

Final Report
December 1991 - July 1995

PHILLIPS LABORATORY
Directorate of Geophysics
AIR FORCE MATERIEL COMMAND
HANSCOM AFB, MA 01731-3010

"This technical report has been reviewed and is approved for publication"

CLAIRE M. DAIGLE
Contract Manager
Space Particlces Env. Branch
Space Physics Division

EDWARD G. MULLEN, Chief
Space Particles Env. Branch
Space Physics Division

WILLIAM SWIDER
Deputy Director
Space Physics Division

This report has been reviewed by the ESC Public Affairs Office (PA) and is releasable to the National Technical Information Service (NTIS).

Qualified requestors may obtain additional copies from the Defense Technical Information Center. All others should apply to the National Technical Information Service.

If your address has changed, or if you wish to be removed from the mailing list, or if the addressee is no longer employed by your organization, please notify PL/TSI, 29 Randolph Road, Hanscom AFB, MA 01731-3010. This will assist us in maintaining a current mailing list.

Do not return copies of this report unless contractual obligations or notices on a specific document requires that it be returned.

REPORT DOCUMENTATION PAGE

Form Approved
OMB No. 0704-0188

1. AGENCY USE ONLY (Leave blank)	2. REPORT DATE	3. REPORT TYPE AND DATES COVERED
	26 July 1995	Final (December 1991 to July 1995)

4. TITLE AND SUBTITLE

Analyze Data from CRRES Payloads AFGL-701-2/Dosimeter and AFGL-701-4/HEEF

5. FUNDING NUMBERS

Contract Number:
F19628-92-C-0020
PE 62101F
PR 7601
TA 22 WU PM

6. AUTHOR(S)

Frederick A. Hanser

7. PERFORMING ORGANIZATION NAME(S) AND ADDRESS(ES)

Panametrics, Inc.
221 Crescent Street
Waltham, MA 02154-3497

8. PERFORMING ORGANIZATION REPORT NUMBER

9. SPONSORING/MONITORING AGENCY NAME(S) AND ADDRESS(ES)

Phillips Laboratory
29 Randolph Road
Hanscom AFB, MA 01731-3010
Contract Monitor: Claire Daigle/GPSP

10. SPONSORING/MONITORING AGENCY REPORT NUMBER

PL-TR-95-2103

11. SUPPLEMENTARY NOTES

12a. DISTRIBUTION/AVAILABILITY STATEMENT

Approved for public release;
Distribution unlimited.

12b. DISTRIBUTION CODE

13. ABSTRACT *(Maximum 200 words)*

Data analysis procedures for the CRESS payloads AFGL-701-2/Dosimeter and AFGL-701-4/HEEF have been developed. The 701-4/HEEF backup instrument response for electrons was measured extensively. The instrument was calibrated at a Van de Graaff accelerator with electrons from about 0.3 to 2.7 MeV, and the high count rate response to beta source electrons was measured. The results have been included in the data analysis procedures, since the in-orbit 0.3 to 1.0 MeV electron fluxes are sometimes well in excess of the pre-launch expected values. Corrected data from 701-4 and 701-2 give electron fluxes that are in reasonable agreement. The 701-4/HEEF backup instrument was also modified to accommodate the temperature variation of the BGO crystal time constants, and now has good detection efficiency from +30°C to -20°C.

14. SUBJECT TERMS			15. NUMBER OF PAGES
Dosimeter	Electron Dose	Proton Dose	84
Electron Flux	Electron Spectra	Space Radiation	16. PRICE CODE

17. SECURITY CLASSIFICATION OF REPORT	18. SECURITY CLASSIFICATION OF THIS PAGE	19. SECURITY CLASSIFICATION OF ABSTRACT	20. LIMITATION OF ABSTRACT
UNCLASSIFIED	UNCLASSIFIED	UNCLASSIFIED	UNLIMITED

Table of Contents

List of Figures

List of Figures (continued)

List of Tables

List of Tables (continued)

List of Tables (continued)

1. Introduction

The AFGL-701-2/Dosimeter and AFGL-701-4/HEEF (High Energy Electron Fluxmeter) were launched aboard the CRRES spacecraft on July 25, 1990. The Dosimeter is designed to measure radiation doses from electrons and protons behind four (4) different thicknesses of aluminum shielding, while HEEF is designed to measure the differential electron flux in the range of 1 to 10 MeV. HEEF also has some response to electrons above about 0.3 MeV, but this low energy range cannot distinguish electrons from other low energy particles such as protons. The instruments have been described in detail in Reference 1.

The Dosimeter data reduction procedures are described in Section 2, while the HEEF data reduction procedures are described in Section 3. Section 3 also contains the results of additional electron calibration and high intensity beta source tests of HEEF SN/2. Some reduced in-orbit data from CRRES are given in Section 4. Section 5 contains the results of coincidence pulse width changes made to the BGO signal in the backup HEEF, which produces a much higher detection efficiency at low temperatures. Additional modifications which can be made to HEEF to reduce the mass and to shield the front SSD from some of the lower energy electrons are also discussed in Section 5.

2. AFGL-701-2/Dosimeter Data Reduction

2.1 General Method for Data Analysis Procedures

The Dosimeter data format and calibration factors have been given in References 1 and 2. An isometric, cross-sectional view of the Dosimeter is given in Figure 1, while the dome and detector properties are summarized in Table 1. All domes have a LOLET energy deposit range of 0.05 - 1.0 MeV and a HILET range of 1.0 - 10.0 MeV, while the VHLET (nuclear Star) thresholds are as listed in Table 1. The resulting nominal particle energy detection ranges are listed in Table 2, with the VHLET proton energies being the minimum possible to produce a VHLET count.

Table 1: Summary of Dosimeter Dome and Detector Properties

Dome No.	Aluminum Shield		Detector		VHLET E Loss (MeV)
	(mils)	(g/cm^2)	Area (cm^2)	Thickness (microns)	
1	82.5	0.57	0.00815	403	40
2	232.5	1.59	0.0514	434	40
3	457.5	3.14	0.0514	399	40
4	886.5	6.08	1.000	406	75

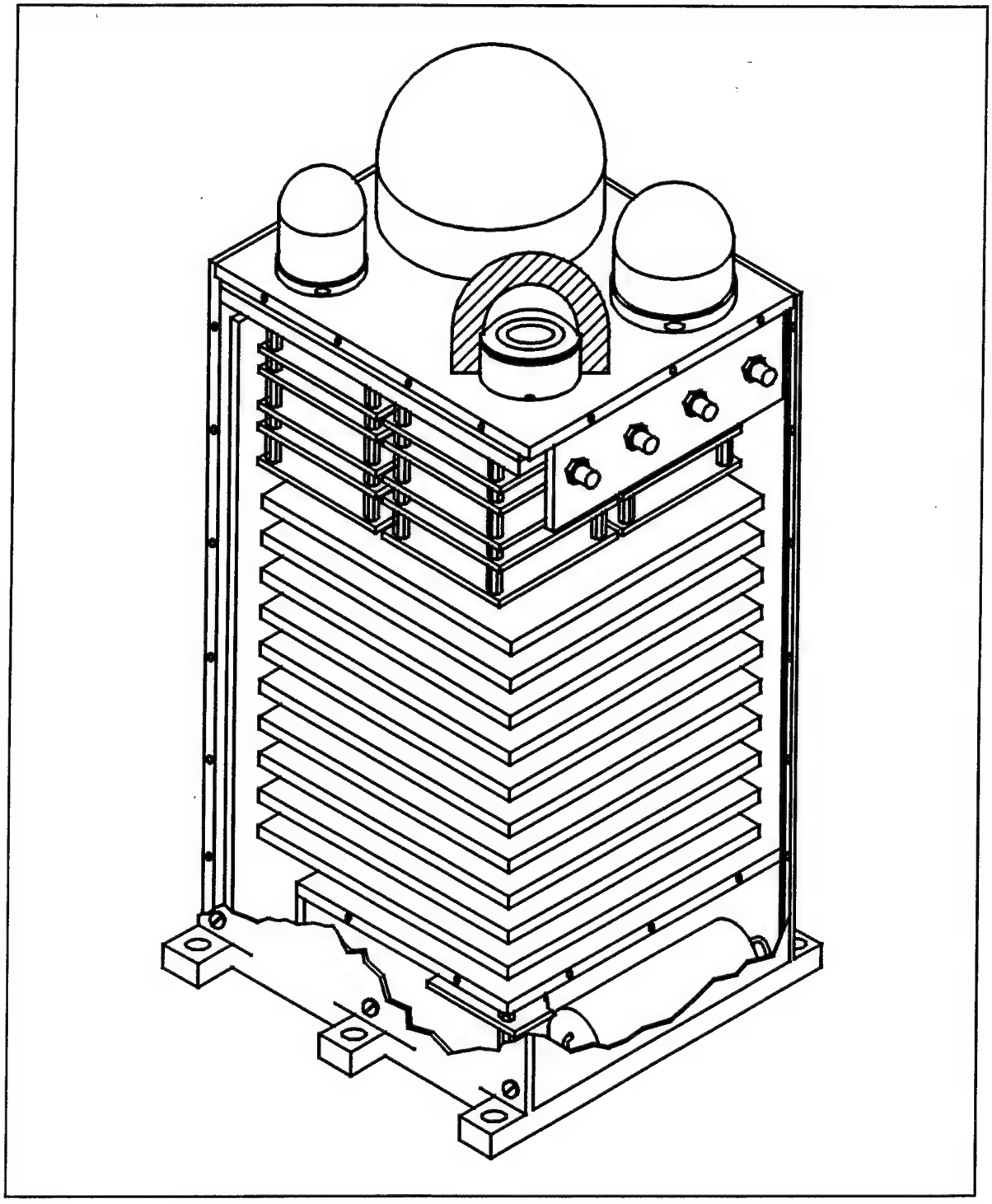

Figure 1. Isometric, Cross-sectional View of the CRRES Dosimeter.

Table 2: Dosimeter Particle Energy Detection Ranges				
Dome No.	LOLET Particles		HILET Protons (MeV)	VHLET Protons (MeV)
	Electrons (MeV)	Protons (MeV)		
1	>1.0	>130	20 - 130	>46
2	>2.5	>135	35 - 135	>56
3	>5.0	>140	51 - 140	>69
4	>10.0	>155	75 - 155	>111

The electron response of the LOLET flux channels has been calibrated at accelerators, and was summarized in Reference 2. The energy dependent electron geometric factors for dome n, in cm^2-sr, are given by the equation

$$\begin{aligned} G_{fen}(E) &= 0 && E/T_n < 1 \\ &= 7.38 \times A_{no} \times (1 - T_n/E) && 1 \le E/T_n \le 3 \\ &= 4.92 \times A_{no} && E/T_n \ge 3 \end{aligned} \qquad (2.1)$$

with the calibrated coefficients being listed in the last two columns of Table 3. The proton geometric factors are to first order given by $\pi \times A$ cm^2-sr, with A being the SSD area in column 2 of Table 3. The proton energy responses vary with the angle of incidence because of the change in path length in the SSD sensitive volume, so the ranges in Table 2 are approximate averages, as are the nominal geometric factors. The remaining items in Table 3 are the prescale factors for the proton (HILET) flux counters, and for the dose counters (electron = LOLET; proton = HILET).

Table 3: Dosimeter Geometric Factor Data						
Dome No.	SSD A (cm^2)	Proton flux prescale	Dose Prescalers		Calib. Electron G_{fe} Constants	
			Electron (K_e)	Proton (K_p)	T_n (MeV)	A_{no} (cm^2)
1	0.00815	1	8192	256	1.0	0.017
2	0.0514	1	8192	1024	2.5	0.075
3	0.0514	1	8192	512	5.0	0.067
4	1.000	8	16384	8192	10.0	0.888

The dosimeter telemetry output consists of 36-bits of data per second, with the four domes cycling through once every 4 seconds. The outputs cycle through 1 NORM A set followed by 15 NORM B sets for a total 64-second cycle for all four domes. A calibration mode is used to shift the LOLET energy loss range to 1-3 MeV and the HILET energy loss range to 3-10 MeV, for measurement of a degraded alpha source during low ambient particle flux periods. The 36-bit data format is listed in Table 4.

The Calibration Mode (CAL MODE) data are all straight binary counters, with the U and L dose and flux counts being compared with pre-launch values to verify SSD total depletion and proper gain. The CAL MODE data are thus only reliable when the ambient particle fluxes are negligible. The NORM MODE data (A and B for a complete set) are used to provide the normal ambient particle data. The fluxes are given by E x M compression counters, with the minimum input count being given by

$$C_{min} = M \times 2^E \qquad (2.2)$$

The electron (LOLET) flux counters are E x M = 4 x 4, while the proton (HILET) flux counters are E x M = 5 x 3. The channel 4 HILET flux has a prescale of 8, as shown in Table 3. The star (VHLET) counters are straight binary.

The LOLET and HILET dose counters provide an accumulated total dose count of

$$\begin{aligned} D &= 16\ n + R + 16\ M\ 2^E, \qquad E \le 7;\ 0 \le n \le 2^E - 1 \\ &= 16\ n + R + 16\ (M + 8(E-7)) \times 128, \qquad E > 7;\ 0 \le n \le 127 \end{aligned} \qquad (2.3)$$

where E is the exponent read out in the NORM A mode, M = m4 m3 m2 m1 is the summed mantissa from the NORM A and B modes, and R is the 4-bit ripple counter from the NORM B mode. The R counter overflow number, n, must be determined by counting R overflows from the preceding E increment. For periods where the dose rate is high enough to result in overflows in R for each readout, it is best to keep a running average of the ratio of R to particle flux, and use this to calculate the number of R overflows in each readout. The overflow count can be checked at the next mantissa increment, since there must be a total of 2^E overflows for a mantissa increment.

The dose prescalers listed in Table 3 are used to derive the actual energy deposit in the SSD's in terms of keV/(flux count). The dose count calibration factors, in Rads(Si)/(output dose count = D), and the average energy (keV) per dose pulse, are listed in Table 5. Note that the output dose count D is used directly to get the Rads(Si) doses (or dose increments), while the dose prescalers in Table 3 must be used along with the dose D to get the keV dose and dose increment. The keV dose increment is then divided by the flux count to get the keV/(flux count) value. This last value can be of use in distinguishing LOLET doses that are from electrons, from high energy protons, and from bremsstrahlung.

Table 4: Dosimeter Telemetry Bit Data Assignment					
Bit	Meaning				
1	Normal Mode ID: 0 = NORM A MODE; 1 = NORM B MODE				
2	Cal Mode ID: 0 = NORM A or B MODE; 1 = CAL MODE				
3	Channel (Dome) ID: 0 = Channel 2, 3, or 4; 1 = Channel 1				
NORM A MODE Bits 1-3 = 00X		NORM B MODE Bits 1-3 = 10X		CAL MODE Bits 1-3 = X1X	
Bits	Meaning	Bits	Meaning	Bits	Meaning
4-7	P dose/E	4-5	P dose/m2,m1	4-11	U CAL dose
8-9	P dose/m4,m3	6-9	P dose/R	12-19	L CAL dose
10-13	E dose/E	10-11	E dose/m2,m1	20	Star flux
14-15	E dose/m4,m3	12-15	E dose/R	21-28	U CAL flux
16-20	Star flux	16-20	Star flux	29-36	L CAL flux
21-23	P flux/E	21-23	P flux/E		
24-28	P flux/M	24-28	P flux/M		
29-32	E flux/E	29-32	E flux/E		
33-36	E flux/M	33-36	E flux/M		

Table 5: Dose Calibration Factors for the CRRES Dosimeter				
Channel (Dome)	Dose Calibration Factors Rads(Si)/(output count)		SSD Calibration keV/(dose pulse)	
	Electron	Proton	LOLET	HILET
1	1.18×10^{-2}	3.24×10^{-3}	68.7	604.
2	1.85×10^{-3}	1.93×10^{-3}	72.9	607.
3	1.16×10^{-3}	1.04×10^{-3}	67.2	601.
4	2.00×10^{-4}	8.30×10^{-4}	72.0	597.

The Dosimeter also has a weak response to low energy electrons from bremsstrahlung production. The bremsstrahlung response for the DMSP/F7 Dosimeter were calculated approximately and given in Appendix A of Reference 7. The Reference 7 calculations can be adjusted to the CRRES Dosimeter by multiplying the Reference 7 responses by the ratio of the CRRES and DMSP/F7 SSD areas for the dome in question. The CRRES Dosimeter bremsstrahlung responses have also been calculated in Reference 8, which used a Monte Carlo integration code. The calculated results from References 7 and 8 are in reasonable agreement, and are summarized in Table 6.

Table 6: Calculated CRRES Dosimeter Electron Bremsstrahlung Responses

Dome	E_e (MeV)	G_{omni} (cm^2)		G (cm^2 sr) Ref. 8	$\frac{4\pi\ G_{omni}}{G}$ (CRRES)	ΔE_{avg} (keV) (Ref. 7)	ΔE_{avg} (keV) (Ref. 8)
		Ref. 7	CRRES				
1	0.2	1.26×10^{-7}	2.00×10^{-8}	2.45×10^{-7}	1.03	68.	83.
1	0.3	2.30×10^{-7}	3.65×10^{-8}	5.76×10^{-7}	0.80	71.	84.
1	0.5	4.85×10^{-7}	7.69×10^{-8}	1.58×10^{-6}	0.61	81.	83.
1	1.0	1.21×10^{-6}	1.92×10^{-7}	9.12×10^{-5}*	0.026*	96.	88.
2	0.2	2.15×10^{-6}	1.11×10^{-7}	7.98×10^{-7}	1.75	69.	71.
2	0.3	3.98×10^{-6}	2.05×10^{-7}	2.00×10^{-6}	1.29	72.	73.
2	0.5	8.58×10^{-6}	4.41×10^{-7}	5.17×10^{-6}	1.07	82.	78.
2	1.0	2.20×10^{-5}	1.13×10^{-6}	1.98×10^{-5}	0.72	98.	94.
3	0.2	1.71×10^{-6}	8.79×10^{-8}	3.56×10^{-7}	3.10	69.	77.
3	0.3	3.27×10^{-6}	1.68×10^{-7}	2.89×10^{-6}	0.73	73.	84.
3	0.5	7.29×10^{-6}	3.75×10^{-7}	6.65×10^{-6}	0.71	85.	92.
3	1.0	1.94×10^{-5}	9.97×10^{-7}	1.89×10^{-5}	0.66	101.	102.
4	0.2	1.10×10^{-6}	1.10×10^{-6}	5.59×10^{-6}	2.47	71.	88.
4	0.3	2.22×10^{-6}	2.22×10^{-6}	1.26×10^{-5}	2.21	75.	91.
4	0.5	5.33×10^{-6}	5.33×10^{-6}	4.54×10^{-5}	1.48	89.	94.
4	1.0	1.52×10^{-5}	1.52×10^{-5}	2.11×10^{-4}	0.91	107.	109.

* The Reference 8 response includes some direct electron penetration, and so is larger than the pure bremsstrahlung calculations of Reference 7.

2.2 Dosimeter Deadtime Corrections

The electron fluxes below and near 1 MeV increased substantially near CRRES orbit 600, and this resulted in the Dosimeter channel 1 sometimes having a count rate high enough to produce significant deadtime effects. The maximum deadtime effect that had been expected from pre-launch calculations was about 7%, but data from L = 4.5 on orbit 600 give a deadtime correction factor of about 1.65. The following method allows the Dosimeter data to be corrected for the deadtime effects for all flux count

and delta-dose readouts, and is applicable to all channels.

For a given readout from the Dosimeter there are four (4) numbers that are required:

C_{fe} = the LOLET (electron) flux count

C_{fp} = the HILET (proton) flux count

D_{de} = the LOLET (electron) <u>delta</u> dose count

D_{dp} = the HILET (proton) <u>delta</u> dose count

The count time interval DT is fixed at 4 seconds for each channel. From the above the following count rates are calculated:

$$\begin{aligned} R_{fe} &= C_{fe} \;/\; DT \\ R_{fp} &= C_{fp} \;/\; DT \\ R_{de} &= D_{de} \;/\; DT \\ R_{dp} &= D_{dp} \;/\; DT \end{aligned} \qquad (2.4)$$

The deadtime fraction is then calculated from

$$T_d = [11 \times (R_{fe} + R_{fp}) + K_e \times R_{de} + K_p \times R_{dp}] \times 10^{-6} \qquad (2.5)$$

and the deadtime correction factor from

$$F_{dt} = 1 \;/\; (1 - T_d) \qquad (2.6)$$

The deadtime corrected counts (or count rates) are then calculated from

$$\begin{aligned} C_{fe,cr} &= C_{fe} \times F_{dt} \\ C_{fp,cr} &= C_{fp} \times F_{dt} \\ D_{de,cr} &= D_{de} \times F_{dt} \\ D_{dp,cr} &= D_{dp} \times F_{dt} \end{aligned} \qquad (2.7)$$

Note that the total dose increments must be added to give the true total dose accumulation, since the dosimeter total dose numbers will not be incremented correctly because of the deadtime factor F_{dt} being larger than 1. The dose prescale factors K_e and K_p used in the above equation are given in Table 3. Note that the proton flux count C_{fp} for channel 4 has a prescale of 8, and this must be used for the channel 4 deadtime calculations. In practice, however, only channel 1 shows a significant deadtime effect and is the only channel which need be corrected.

An example of the effect is given in orbit 600, at L = 4.48, for a UT range of 14657 to 14694 seconds. The channel 1 average

count outputs are

$$C_{fe} = 110592., \qquad R_{fe} = 27648.\ s^{-1}$$
$$C_{fp} = 39.6, \qquad R_{fp} = 9.9\ s^{-1}$$
$$D_{de} = 43.0, \qquad R_{de} = 10.75\ s^{-1} \tag{2.8}$$
$$D_{dp} = 0.4, \qquad R_{dp} = 0.1\ s^{-1}$$

which give

$$T_d = 0.3923 \tag{2.9}$$

and

$$F_{dt} = 1.646 \tag{2.10}$$

This is a significant deadtime factor, and must be used to provide better flux and delta dose values for channel 1. The delta dose values must then be summed to provide the true corrected total dose for channel 1, both LOLET and HILET.

3. AFGL-701-4/HEEF Calibration and Data Reduction

3.1 Description of HEEF

A schematic cross-sectional view of HEEF is given in Figure 2, which shows the geometrical arrangement of the two solid state detectors (SSD's) and the Bismuth Germanate (BGO) scintillator. The anti-coincidence plastic scintillator surrounds the electron energy-measuring BGO scintillator to eliminate any particles which exit the BGO without losing all of their energy. Normal HEEF operation requires a triple coincidence between the two SSD's and the BGO, and an anti-coincidence with the plastic scintillator. The energy loss curves for electrons and protons in the SSD's and BGO have been plotted in Reference 1.

The SSD pulse amplitudes required for the several single count outputs are listed in Table 7. These counts are telemetered as part of the HEEF data to verify instrument operation and to allow correction for deadtime effects when necessary. The nominal particle responses neglect the spread in the energy loss of the particles, particularly the electrons.

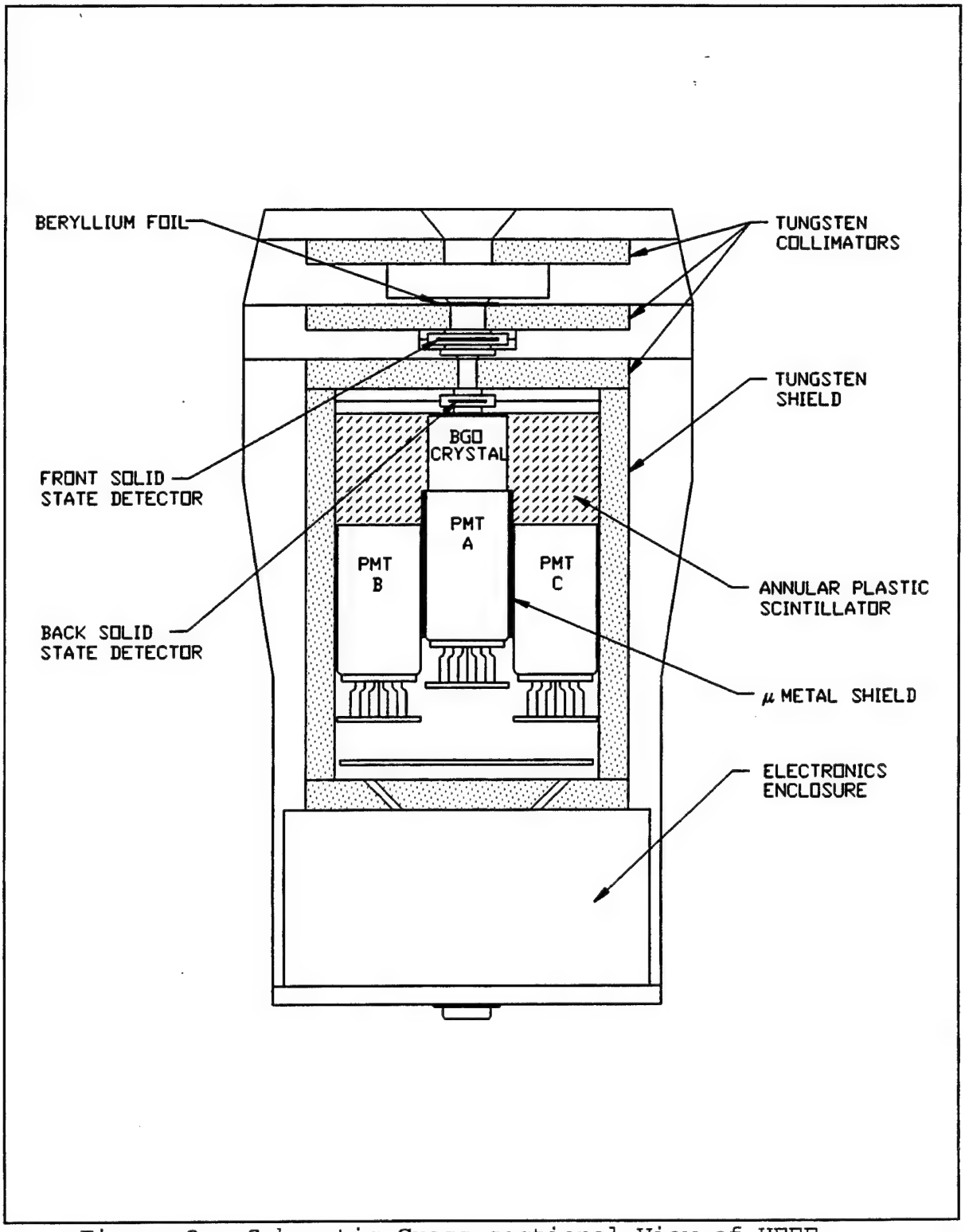

Figure 2. Schematic Cross-sectional View of HEEF.

Table 7: HEEF Solid State Detector Energy Losses				
Channel and SSD	Count Designation	SSD Energy Loss (MeV)	Primary Energy Response (MeV)	
			Electrons	Protons
>S2, Front SSD	S2F	>0.80	---	4.2-130
>S1, Front SSD	S1F	>0.50	---	4.1-270
W1, Front SSD	W1F	0.13-0.50	>0.2	>270
W2, Front SSD	W2F	0.13-0.80	>0.2	>130
>S2, Back SSD	S2B	>0.80	---	11.2-130
>S1, Back SSD	S1B	>0.50	---	11.1-270
W1, Back SSD	W1B	0.13-0.50	>0.5	>270
W2, Back SSD	W2B	0.13-0.80	>0.5	>130

The primary electron channel response from the triple coincidence mode is given in Table 8. This response is for when the BGO scintillator gain is set correctly, and shifts for different gains. The "Count Designation" in Tables 7 and 8 give the abbreviated notations used in this report for the telemetered count data from HEEF. Table 8 lists the triple coincidence requirements for the electron channels. Note that the four (4) lowest energy channels use the W2F/W2B SSD windows, while the higher energy channels use the W1F/W1B SSD windows. The L10C channel is an integral response channel for electrons above 10 MeV and protons above about 270 MeV. The listed primary energy responses are nominal values based on the energy loss calculations for the particles in question.

3.2 Calibration with Electrons at a Van de Graaff Accelerator

The HEEF SN/2 was calibrated at a Van de Graaff accelerator located in building N10 at MIT. The calibration went up to about 3 MeV, with the beam having a reasonably broad irradiation area and a narrow energy range. This provided a more reliable calibration than those of HEEF SN/1 at the NASA/GSFC Van de Graaff and at the RADC Linear Accelerator (References 3, 4).

3.2.1 Set-up and Data Analysis Method

The geometry of the calibration set-up at the MIT Van de Graaff is shown in Figure 3. The HEEF SN/2 was positioned on a rotating table about 25 inches from the exit window of the 90° analyzing magnet vacuum pipe, with two monitor detectors M1 and M2 positioned as shown. The monitor detectors had precise collimators to measure the true electron beam intensity. Since the monitors were placed at the sides and in front of HEEF, a correction had to be made for the electron beam intensity distribution in both

Table 8: HEEF Primary Channel Energies				
BGO Channels and SSD Coincidences	Count Designation	BGO Energy Loss (MeV)	Primary Energy Response (MeV)	
			Electrons	Protons
LL-L1/W2F/W2B	LL	0.44-0.96	1.0-1.5	---
L1-L2/W2F/W2B	L1	0.96-1.46	1.5-2.0	---
L2-L3/W2F/W2B	L2	1.46-1.96	2.0-2.5	---
L3-L4/W2F/W2B	L3	1.96-2.45	2.5-3.0	---
L4-L5/W1F/W1B	L4	2.45-2.95	3.0-3.5	---
L5-L6/W1F/W1B	L5	2.95-3.44	3.5-4.0	---
L6-L7/W1F/W1B	L6	3.44-4.43	4.0-5.0	---
L7-L8/W1F/W1B	L7	4.43-5.42	5.0-6.0	---
L8-L9/W1F/W1B	L8	5.42-7.41	6.0-8.0	---
L9-L10/W1F/W1B	L9	7.41-9.40	8.0-10.0	---
>L10/W1F/W1B	L10C	>9.40	>10.0	>270

distance and angle. The corrections were derived from beam scans made with M2, some of which were made with M1 located just in front of the HEEF aperture. The electronics configuration is shown in Figure 4, with HEEF rotations, M2 scans, and data recording all being done outside the beam room. HEEF data and the M1 and M2 SCA (Single Channel Analyzer - integral threshold above 175 keV) counts were recorded simultaneously to avoid problems from beam intensity variations. Detector spectra (M1, M2, SSDF, SSDB, and BGO) were taken periodically during the calibration to provide beam monitoring and energy measurement, as well as to provide data on the electron energy loss spectra in the various detectors.

The Van de Graaff energy was set by using the reading of a digital panel meter on the control console. The beam energy in MeV is nominally twice the reading of the panel meter. The nominal electron beam energy was calibrated using the full-energy loss peaks in M1 and M2. Since M2 was 1500 microns thick (Figure 3) it gave a discernable full-energy peak even for the nominal 3.0 MeV beam. The internal (vacuum) electron energy is degraded by energy loss in the 3-mil thick Al vacuum window after the 90° analyzing magnet, and by the various air paths to M1 (d1), M2 (d2), and HEEF (df) (M2 also has a 0.3-mil thick Al light shield). The HEEF SN/2 electron calibrations were made during a series of runs that involved moving and then repositioning the set-up in the electron beam to allow other Van de Graaff uses between run sets. Table 9 summarizes the run sets made, along with the detector distances shown in Figure 3. The HEEF SN/2 data file name listed is for the data recorded by the GSE computer. The monitor detector counts for the various record numbers were written into a Laboratory Notebook

(FLUX 4 SN/002). MITCAL.001 was a preliminary test verifying beam control and checking detector responses. The M1 monitor was added for later runs since it was found that the electron beam intensity generally varied with time, and M1 is thus needed for normalization to allow M2 to scan in front of HEEF and make a correct beam profile scan.

The electron beam energy calibration was made from the M2 MCA (Multi Channel Analyzer) data taken during the MITCAL.005 runs. The M2 gain was calibrated with the 477.3 keV Compton edge from the 661.6 keV gamma rays from a weak Cs-137 source. The MCA linearity and zero pulse height channel were measured using a precision Research Pulser. The M2 full energy loss peak energy for the electrons has to be corrected for the energy loss in the Al foils and the air path. The results are given in the first five columns of Table 10, for all of the energies used (Tr-Nom is the difference between the true electron energy in vacuum and the nominal value). Energy losses for the electrons were calculated using the tables for aluminum and air in Reference 6. The data from columns 1 and 5 in Table 10 are plotted in the top part of Figure 5, and have a best-fit straight line of

$$(\text{True} - \text{Nominal}) = -0.0782 \times \text{Nominal} + 0.1321 \qquad (3.1)$$

The bottom part of Figure 5 shows the same type of data taken during the Dosimeter calibrations in September, 1992, and show that this Van de Graaff energy calibration is reasonably stable, since the fit for these data is

$$(\text{True} - \text{Nominal}) = -0.0869 \times \text{Nominal} + 0.1425 \qquad (3.2)$$

The two fits give the same true electron energy to ±1.5 keV over the nominal energy range of 0.15 to 3.0 MeV (true electron energy range of 0.12 to 2.90 MeV).

The last two columns in Table 10 give the best fit results for the true electron energy in vacuum, and the effective electron energy for HEEF SN/2 at the 28.25 inch position (the effective average air path length for the HEEF SSDF, SSDB and BGO detectors is about 29 inches). The effective HEEF electron energies in Table 10 are suitable for all of the HEEF MIT data except the MITCAL.001 data, which latter have not been used for the geometric factor calculations.

The electron beam intensity profile was obtained from the M2 scans for most of the energies used. The electrons scatter in the 3 mil Al vacuum window and in the air path to the detectors. The M2 scan data show that the dominant result is a $1/d^2$ variation, with d (d1, d2, or df) being the distance from the vacuum window to the detector. There is also a profile across the beam which is centered on the beam axis (HEEF center). The cross-beam profile varies with energy, being narrower at the higher energies. For most of the calibration data the M2 monitor was about 13 inches in front of and 2 inches to the side of HEEF. The scan data showed

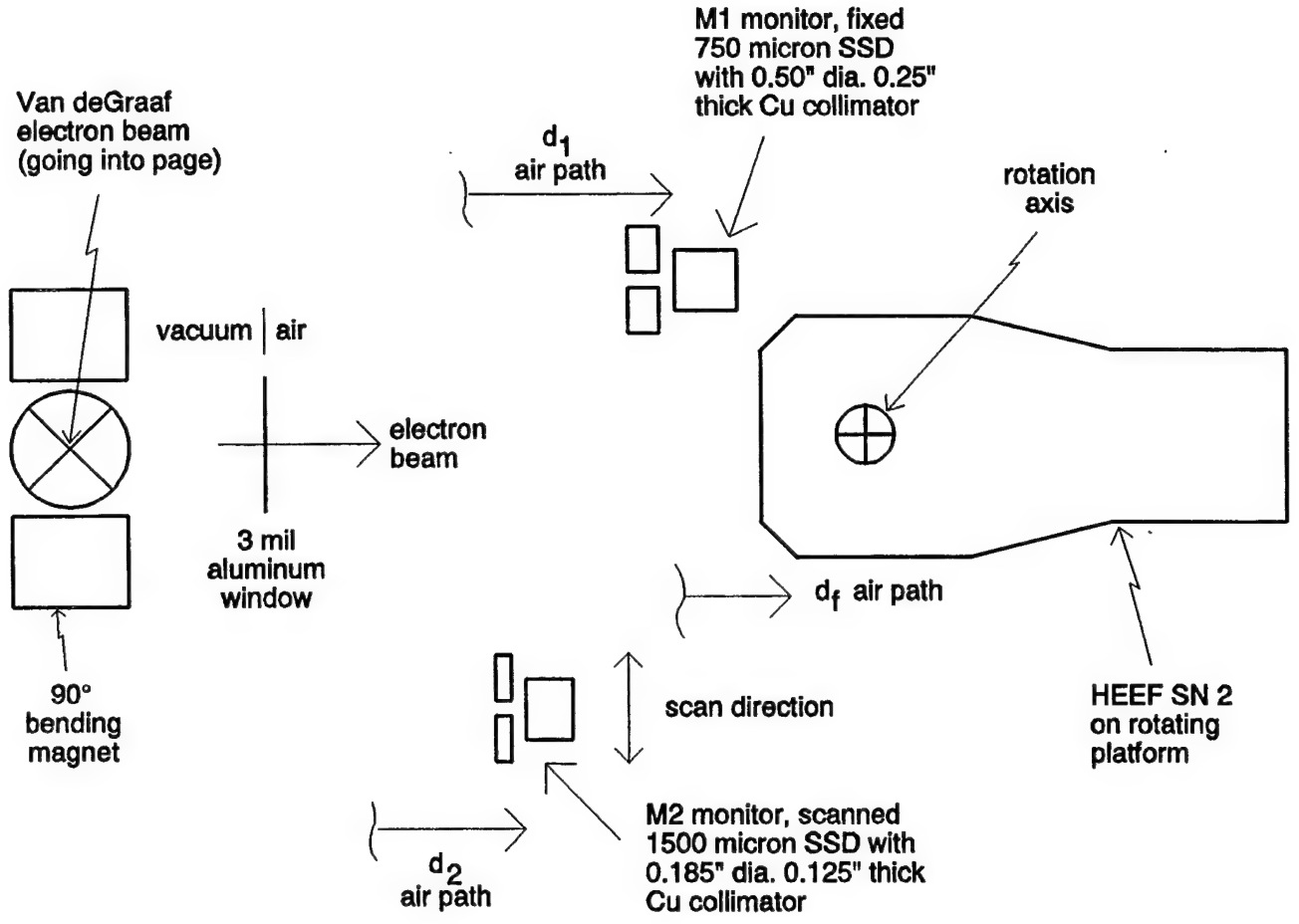

Figure 3. Experimental Configuration for Electron Calibration at the MIT Van de Graaff.

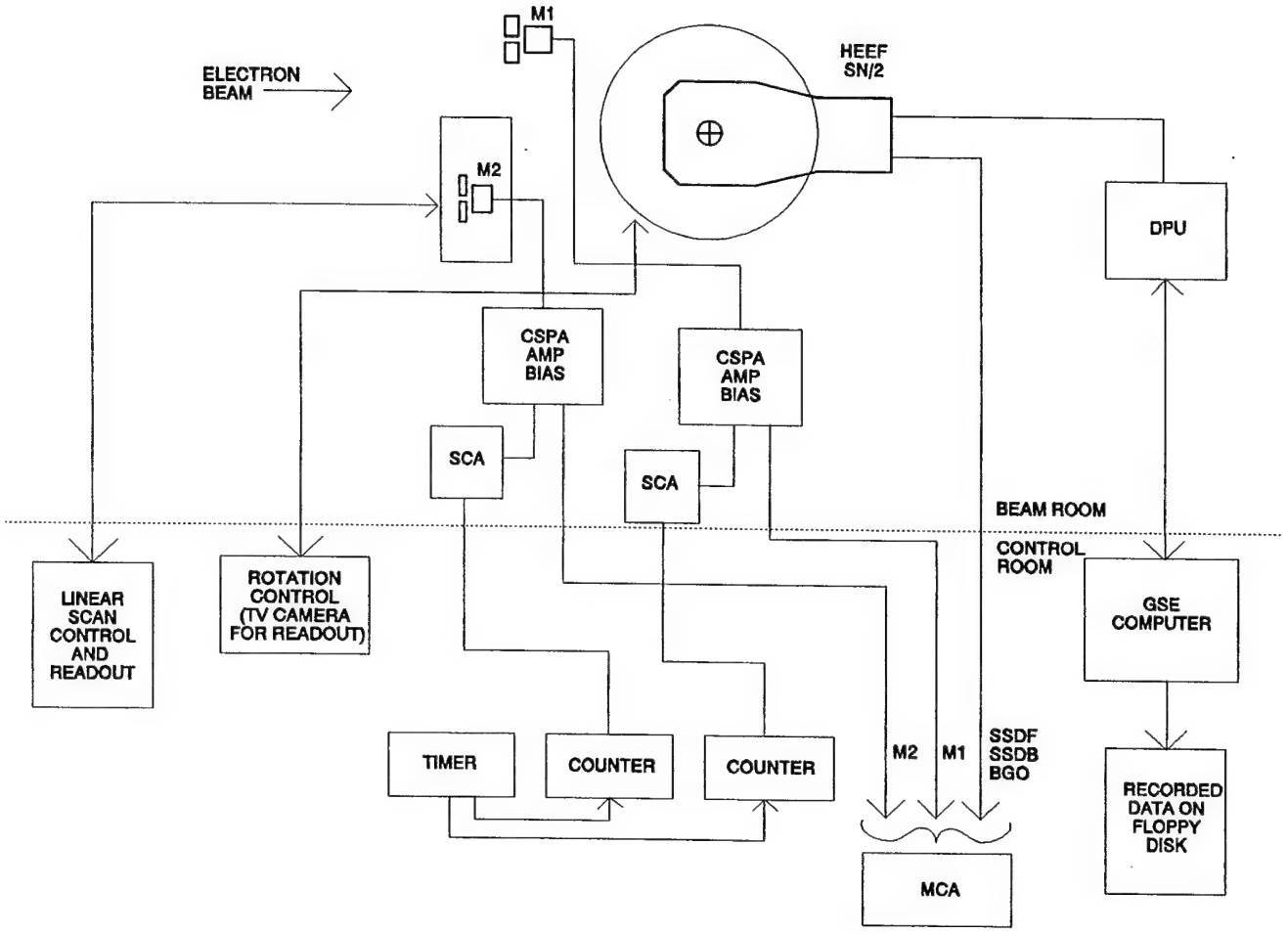

Figure 4. Electronics and Control Configuration for Electron Calibration at the MIT Van de Graaff.

Table 9: Summary of HEEF SN/2 Calibration Run Sets				
HEEF SN/2 Data File	Air path (inches) to front of			Type of Data taken
	M1 (d1)	M2 (d2)	HEEF/SSDF	
MITCAL.001	--	43	56	HEEF/rot; M2/scan
MITCAL.002	25	15.75	28.5	HEEF/rot; M2/scan
MITCAL.003	25	15.75	28.5	HEEF/rot
MITCAL.004	24.75	15.25	28.25	HEEF/rot; M2/scan
MITCAL.005	24.75	15.25	28.25	HEEF/rot; M2/scan
"	25.25	15.25	--	M2/scan; M1 at HEEF
"	26.5	15.25	28.25	HEEF/coinc; M2/scan

that because of electron scattering in the air, for these data the HEEF was partially shielded by the M2 mount. The HEEF data were corrected for this effect by shielding factors derived from the full M2 scan data by comparing the SSDF and M2 count rates against the M1 count rate for beam intensity normalization.

The HEEF counts were converted to a calibrated area by

$$A(cnt) = cnt/(T_{cnt} \times F_e) \quad cm^2 \tag{3.3}$$

where

$$F_e = (cnt_{M2}/T_{M2}) \times GF_{M2} \quad el/(cm^2\ s) \tag{3.4}$$

and

$$GF_{M2} = (d2/df)^2/(A_{M2} \times (M2/HEEF)_{cal} \times (M2\ shldng\ fact)) \quad cm^{-2} \tag{3.5}$$

with a similar equation for the M1 monitor. The symbols are defined as (d2, df, and d1 are defined in Figure 3 and Table 9)

cnt = sum of HEEF channel counts (S1F, W1F, LL, etc.)
T_{cnt} = total accumulation time for cnt - usually 8.192 s
cnt_{M2} = M2 monitor count
T_{M2} = time for accumulation of cnt_{M2} - usually 10 s
A_{M2} = area of collimator for M2 monitor = 0.173 cm^2
$(M2/HEEF)_{cal}$ = calibrated scan intensity ratio at M2 vs. HEEF
= 1.059 for M2 at 2 inches off axis (except taken as = 1.00 for MITCAL.001)
(M2 shldng fact) = calibrated shielding factor of M2 for HEEF

The GF_{M2} and GF_{M1} factors for the data with M2 at 2 inches to the side of HEEF are listed in Table 11 for M2 and Table 12 for M1. All HEEF angular rotation data were taken with M2 in this location. The factors vary with energy as shown. HEEF data were typically

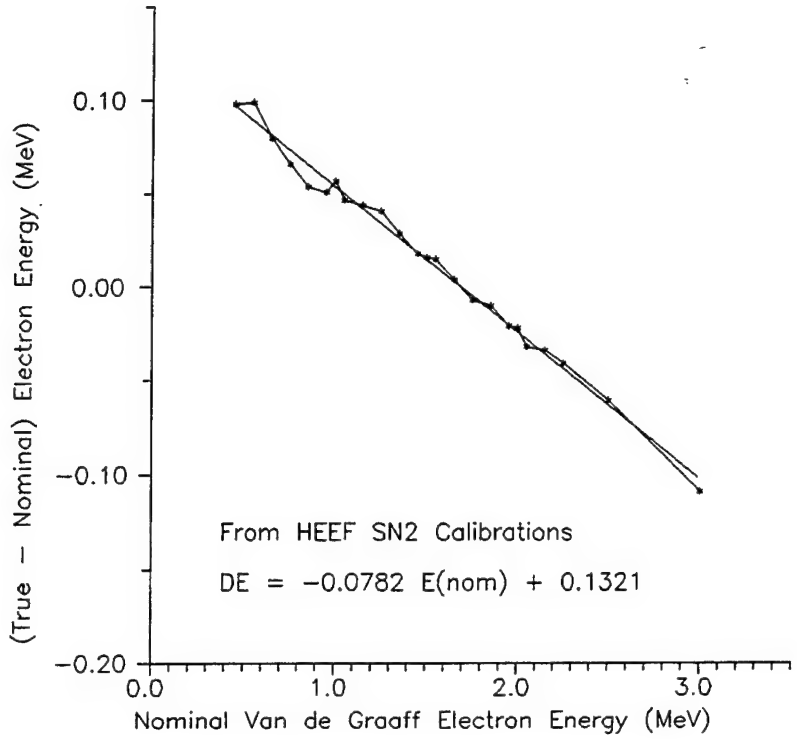

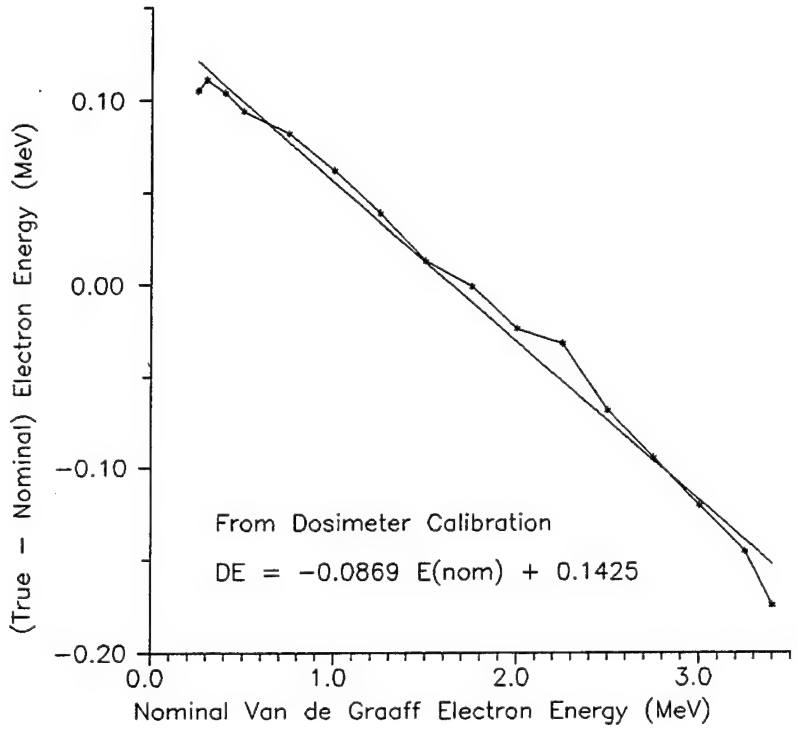

Figure 5. Electron Energy Calibration of the MIT Van de Graaff.

Table 10: Electron Energy Calibration for HEEF SN/2 Calibration						
Nominal (MeV)	M2 Meas (MeV)	Total E Loss (MeV)		Meas Tr-Nom E (MeV)	Best Fit True Energy (MeV)	
		To M2	To HEEF		In Vac	At HEEF
0.45	0.423	0.125	0.194	0.098	0.547	0.35
0.55	0.528	0.121	0.192	0.099	0.639	0.45
0.65	0.613	0.117	0.185	0.080	0.731	0.55
0.75	0.701	0.115	0.183	0.066	0.823	0.64
0.85	0.790	0.114	0.181	0.054	0.916	0.74
0.95	0.887	0.114	0.181	0.051	1.008	0.83
1.00	0.943	0.114	0.181	0.057	1.054	0.87
1.05	0.983	0.114	0.181	0.047	1.100	0.92
1.15	1.080	0.114	0.181	0.044	1.192	1.01
1.25	1.177	0.114	0.181	0.041	1.284	1.10
1.35	1.265	0.114	0.181	0.029	1.377	1.20
1.45	1.354	0.114	0.181	0.018	1.469	1.29
1.50	1.402	0.114	0.181	0.016	1.515	1.33
1.55	1.451	0.114	0.181	0.015	1.561	1.38
1.65	1.539	0.115	0.183	0.004	1.653	1.47
1.75	1.628	0.115	0.183	-0.007	1.745	1.56
1.85	1.725	0.115	0.183	-0.010	1.837	1.65
1.95	1.814	0.115	0.183	-0.021	1.930	1.75
2.00	1.862	0.116	0.184	-0.022	1.976	1.79
2.05	1.902	0.116	0.184	-0.032	2.022	1.84
2.15	1.999	0.117	0.185	-0.034	2.114	1.93
2.25	2.092	0.117	0.185	-0.041	2.206	2.02
2.50	2.321	0.118	0.187	-0.061	2.437	2.25
3.00	2.770	0.121	0.192	-0.109	2.897	2.71

recorded for 2 GSE records of 8 × 0.512 s accumulation time counts, for a total accumulation time of 8.192 s. The M2 and M1 counts were typically accumulated for 10 s. The (M2 shldng fact) calibrated values are listed in Table 13.

The various HEEF channel geometric factors were calculated from the measured $A(\theta)$ values (θ is the angle for the cnt used in the equation above) by

$$G = \sum A(\theta_i)\ \Omega(\theta_i) \quad cm^2\ sr \tag{3.6}$$

where

$$\Omega(\theta_i) = 2\pi \left(\cos(\theta_i - \Delta\theta_{i-}/2) - \cos(\theta_i + \Delta\theta_{i+}/2)\right) \quad \text{sr} \qquad (3.7)$$

with $\Delta\theta_{i-} = \theta_i - \theta_{i-1}$, $\Delta\theta_{i+} = \theta_{i+1} - \theta_i$. Note that for i = 1, $\Delta\theta_{i-} = 0$, and for i = max, $\Delta\theta_{i+} = \Delta\theta_{i-}$.

Table 11: M2 Monitor Calibration Constants for HEEF Data

Nom Electron Energy Range (MeV)	GF_{M2} Factor for HEEF Data File MIT+				
	CAL.001	CAL.002	CAL.003	CAL.004	CAL.005
0.45 - 0.65	3.02	1.48	1.48	1.41	1.41
0.75 - 0.85	2.99	1.46	1.46	1.40	1.40
0.95 - 1.15	2.89	1.41	1.41	1.35	1.35
1.25 - 3.00	2.66	1.30	1.30	1.24	1.24

Table 12: M1 Monitor Calibration Constants for HEEF Data

Nom Electron Energy Range (MeV)	GF_{M1} Factor for HEEF Data File MIT+				
	CAL.001	CAL.002	CAL.003	CAL.004	CAL.005
0.45 - 0.65	---	0.507	0.507	0.506	0.506
0.75 - 0.85	---	0.503	0.503	0.502	0.502
0.95 - 1.15	---	0.486	0.486	0.485	0.485
1.25 - 3.00	---	0.448	0.448	0.447	0.447

Table 13: M2 Shielding Factor for HEEF

Nominal Electron Energy Range (MeV)	(M2 shldng fact)
0.55	1.13
0.75	1.14
1.00	1.18
1.25 - 3.00	1.28

3.2.2 Calibrated Electron Response of HEEF SN/2

The calibration results for HEEF SN/2 for the total BGO PMT counts (summed over all channels) in the triple coincidence mode is given in Table 14. Also given is the measured area for SSDF, based on the M1 and M2 areas normalized for the beam distribution. The measured SSDF area exceeds the HEEF front collimator area for the nominal 2.5 and 3.0 MeV beams, but both of these beams were narrow because of the reduced electron scattering, and both also had some large beam intensity fluctuations from Van de Graaff dark currents (the 3.0 MeV beam was especially bad in this regard). The HEEF

Table 14: HEEF SN/2 Calibrated Electron Coincidence Response

Electron Beam Energy (MeV)		SSDF A(0°) (cm^2) (0.732 max)	PMT total coinc. counts	
VdG Nom	Cal/Eff		Area(0°) (10^{-4} cm^2)	G Factor (10^{-5} cm^2 sr)
0.45	0.35	0.173	0.0	0.0
0.55	0.45	0.241	0.0	0.0
0.65	0.55	0.323	0.0	0.0
0.75	0.64	0.391	0.0	0.0
0.85	0.74	0.459	0.0	0.0
1.00	0.87	0.475	0.074	0.278
1.05	0.92	0.512	0.566	1.588
1.15	1.01	0.580	3.23	7.74
1.25	1.10	0.725	11.95	31.7
1.35	1.20	0.638	18.6	42.0
1.45	1.29	0.657	29.2	69.9
1.50	1.33	0.760	36.3	84.6
1.55	1.38	0.679	38.4	92.2
1.65	1.47	0.689	50.3	115.3
1.75	1.56	0.761	66.8	151.4
1.85	1.65	0.832	86.5	201.
1.95	1.75	0.813	104.6	213.
2.05	1.84	0.756	113.4	261.
2.15	1.93	0.731	128.3	266.
2.25	2.02	0.726	145.	292.
2.50	2.25	1.092*	255./171.	503./337.
3.00	2.71	1.362*	437./232.	772./410.

* The BGO responses have been corrected to an area of 0.732 cm^2 for SSDF.

responses for nominal 2.5 and 3.0 MeV electrons were thus normalized to give an area for SSDF of 0.732 cm^2. The total PMT G factors for the triple coincidence (summed LL, L1, L2, L3 and L4 counts) are plotted in Figure 6 along with the NASA/GSFC Van de Graaff and the RADC Linear Accelerator calibration data for HEEF SN/1 (Reference 3, updated in Reference 4). The calibrations for HEEF's SN/1 and SN/2 agree well in shape, but the absolute values differ by about a factor of two.

The measured geometric factors for the triple coincidence electron channels for HEEF SN/2 are listed in Table 15 and plotted in Figure 7, which also shows the total geometric factor plotted in Figure 6. Note that because of the rapid rise of the total geometric factor up to about 1.5 - 2 MeV, the LL-L1 G-factor is more like a step function, being nearly flat for energies above 1.3 MeV. Only the higher energy channels have a true peak in the G-factor. The LL-L1 channel is thus more like an integral channel for electrons above about 1.1 MeV.

Table 15: Calibrated Electron Channel Geometric Factors for HEEF SN/2

Electron Beam Energy (MeV)		Measured Geometric Factors G (10^{-5} cm^2 sr)				
VdG Nom	Cal/Eff	LL-L1	L1-L2	L2-L3	L3-L4	L4-L5
1.00	0.87	0.28	0.00	0.00	0.00	0.00
1.05	0.92	1.59	0.00	0.00	0.00	0.00
1.15	1.01	7.74	0.00	0.00	0.00	0.00
1.25	1.10	31.6	0.111	0.00	0.00	0.00
1.35	1.20	40.3	1.73	0.00	0.00	0.00
1.45	1.29	61.4	8.53	0.00	0.00	0.00
1.50	1.33	72.5	12.1	0.00	0.00	0.00
1.55	1.38	65.3	26.8	0.058	0.00	0.00
1.65	1.47	65.8	49.3	0.246	0.00	0.00
1.75	1.56	66.0	82.9	2.56	0.00	0.00
1.85	1.65	70.6	118.	11.7	0.00	0.00
1.95	1.75	58.6	116.	37.5	0.00	0.00
2.05	1.84	63.6	110.	87.4	0.507	0.00
2.15	1.93	60.4	87.7	116.	1.96	0.00
2.25	2.02	57.1	77.5	148.	9.20	0.00
2.50	2.25	58.4*	62.6*	161.*	55.2*	0.504*
3.00	2.71	56.2*	56.6*	75.7*	138.*	79.6*

* Corrected to a front SSD area of 0.732 cm^2.

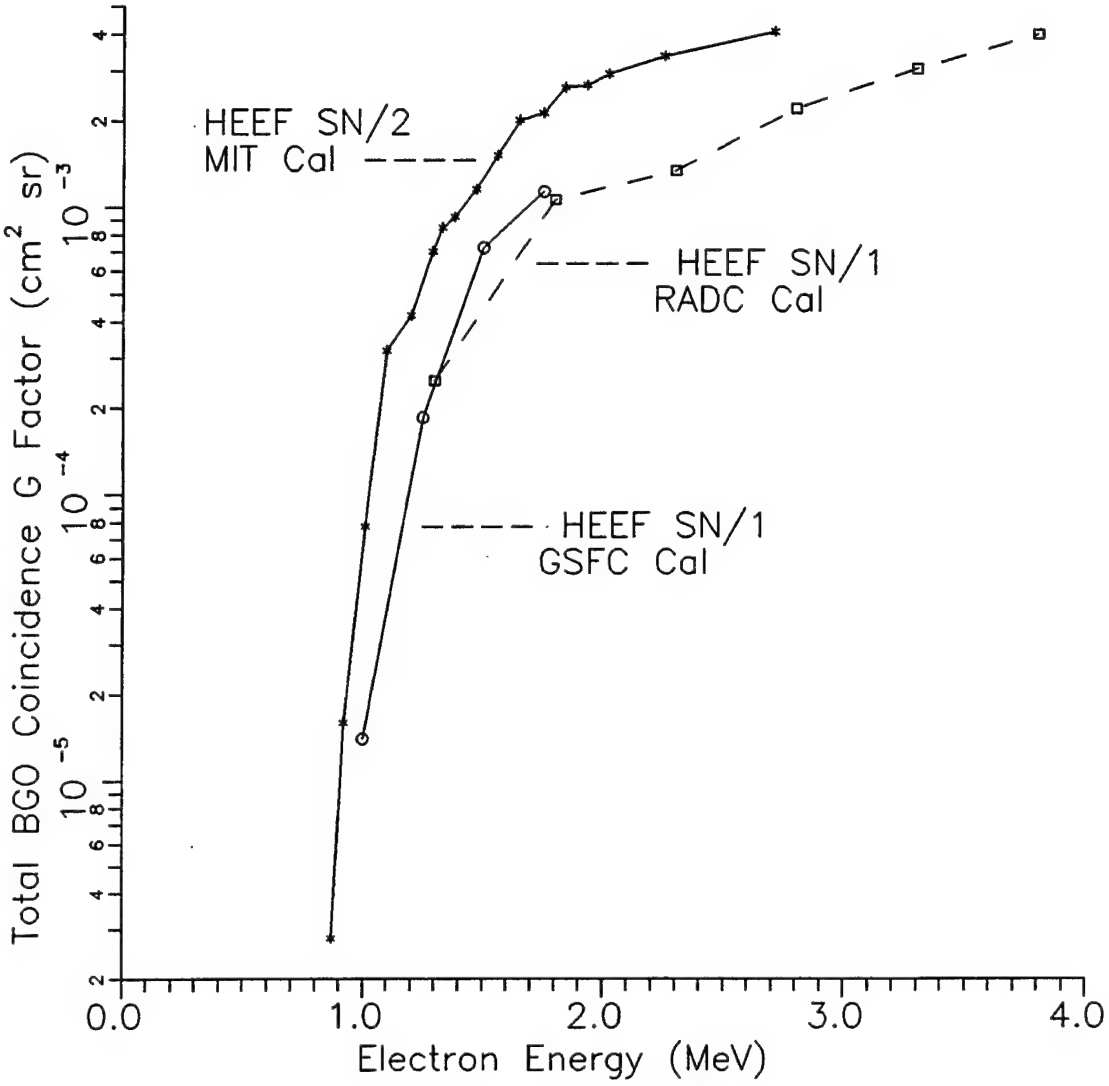

Figure 6. HEEF SN/1 and SN/2 Calibrated Electron Geometric Factors.

The calibrated electron geometric factors for the front (SSDF) and back (SSDB) solid state detector channels are listed in Tables 16 and 17. The G factors are plotted in Figure 8. The various SSDF and SSDB channels act as approximate integral channels for electrons above a threshold energy, except for W1B and W2B which have a slow rise over the range of 0.5 - 3.0 MeV. The energy ranges and best-fit G-factors for the various SSDF and SSDB channels are listed in Table 18. For a moderately steeply falling electron spectrum all channels can be approximated as a single threshold at a fixed energy. For power law spectra of about E^0 to E^{-8} the average value for E_{th} (MeV) and G_o (cm^2 sr) are listed in Table 19.

Table 16: HEEF SN/2 SSDF Calibrated Electron Geometric Factors

Electron Beam Energy (MeV)		Measured Geometric Factors G (10^{-3} cm^2 sr)				
VdG Nom	Cal/Eff	Total	S1F	W1F	S2F	W2F
0.45	0.35	92.8	0.0183	92.8	0.0	92.8
0.55	0.45	112.	0.336	111.	0.007	112.
0.65	0.55	132.	57.4	74.2	0.017	132.
0.75	0.64	153.	87.1	65.7	0.094	153.
0.85	0.74	175.	90.8	84.1	0.192	175.
1.00	0.87	166.	71.6	94.8	27.7	139.
1.05	0.92	177.	70.2	107.	32.4	144.
1.15	1.01	199.	69.1	130.	32.5	166.
1.25	1.10	235.	72.4	163.	33.2	202.
1.35	1.20	196.	53.7	143.	23.9	172.
1.45	1.29	206.	50.6	156.	21.7	184.
1.50	1.33	239.	57.3	182.	24.7	215.
1.55	1.38	205.	45.6	160.	19.2	186.
1.65	1.47	205.	41.8	163.	17.3	186.
1.75	1.56	227.	42.9	185.	17.6	210.
1.85	1.65	252.	43.6	208.	17.4	234.
1.95	1.75	225.	35.2	190.	13.7	211.
2.05	1.84	231.	33.4	197.	12.8	218.
2.15	1.93	213.	29.0	184.	11.0	201.
2.25	2.02	206.	26.3	179.	9.74	196.
2.50	2.25	219.*	29.2*	190.*	11.1*	208.*
3.00	2.71	212.*	28.7*	184.*	10.1*	202.*

* Corrected to a front SSD area of 0.732 cm^2.

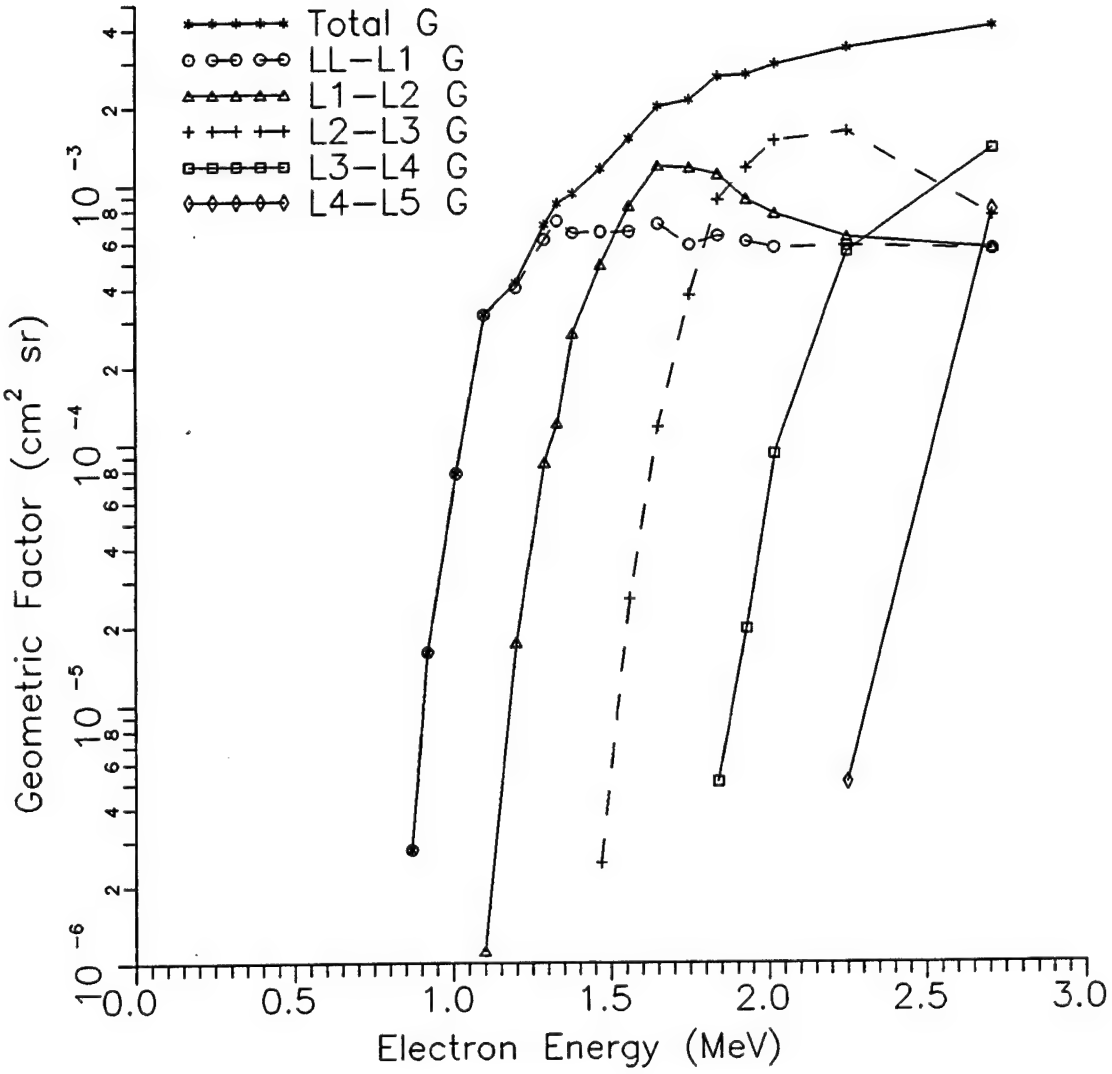

Figure 7. Calibrated Electron Channel Geometric Factors for HEEF SN/2.

The angular response of HEEF SN/2 to electrons was also measured, and is illustrated by the W2F data shown in Figure 9 and the total BGO (triple coincidence) response shown in Figure 10. Most of the HEEF response is for electrons within 20° of the view axis. The measured angular areas must be multiplied by the incremental solid angle factors and summed to give the total geometric factors shown in Figures 6, 7 and 8.

Table 17: HEEF SN/2 SSDB Calibrated Electron Geometric Factors

Electron Beam Energy (MeV)		Measured Geometric Factors G (10^{-3} cm^2 sr)				
VdG Nom	Cal/Eff	Total	S1B	W1B	S2B	W2B
0.45	0.35	0.013	0.0039	0.0090	0.0039	0.0090
0.55	0.45	0.003	0.0003	0.0029	0.00	0.0033
0.65	0.55	0.094	0.0008	0.093	0.00	0.094
0.75	0.64	0.51	0.0004	0.512	0.00	0.512
0.85	0.74	1.23	0.073	1.16	0.00	1.23
1.00	0.87	1.91	0.83	1.08	0.00	1.91
1.05	0.92	2.28	1.13	1.14	0.0009	2.28
1.15	1.01	3.07	1.51	1.56	0.079	2.99
1.25	1.10	4.16	1.93	2.23	0.521	3.64
1.35	1.20	3.81	1.68	2.13	0.617	3.19
1.45	1.29	4.28	1.70	2.58	0.710	3.57
1.50	1.33	5.04	1.98	3.06	0.805	4.23
1.55	1.38	4.58	1.75	2.83	0.735	3.84
1.65	1.47	4.94	1.74	3.20	0.733	4.21
1.75	1.56	5.84	1.96	3.87	0.804	5.03
1.85	1.65	6.83	2.17	4.65	0.889	5.94
1.95	1.75	6.43	1.91	4.53	0.738	5.70
2.05	1.84	7.08	1.97	5.11	0.814	6.26
2.15	1.93	6.74	1.76	4.98	0.659	6.08
2.25	2.02	6.94	1.70	5.24	0.641	6.30
2.50	2.25	9.22*	2.40*	6.82*	1.032*	8.18*
3.00	2.71	10.47*	2.31*	8.16*	0.837*	9.62*

* Corrected to a front SSD area of 0.732 cm^2.

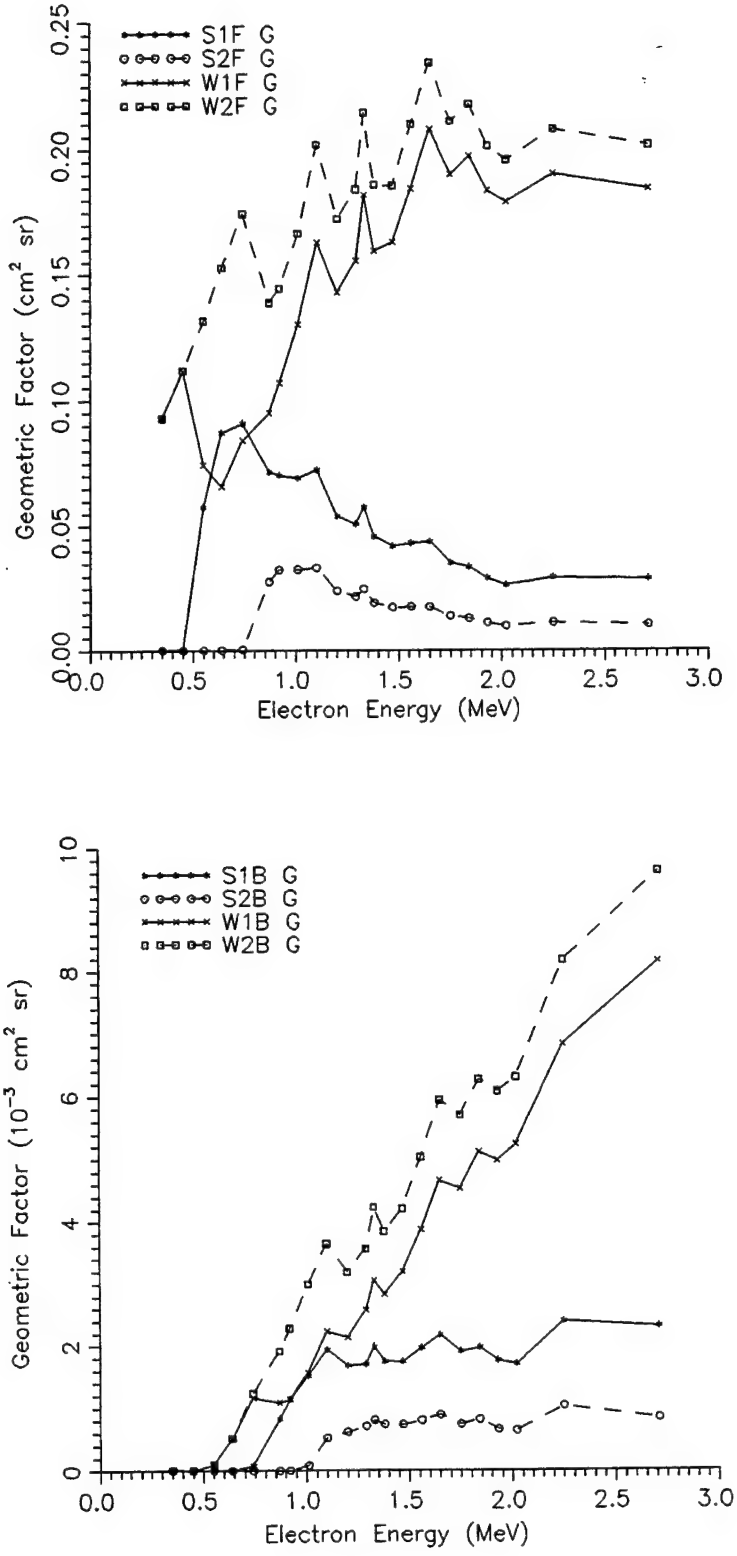

Figure 8. HEEF SN/2 Calibrated Electron Geometric Factors for SSDF and SSDB.

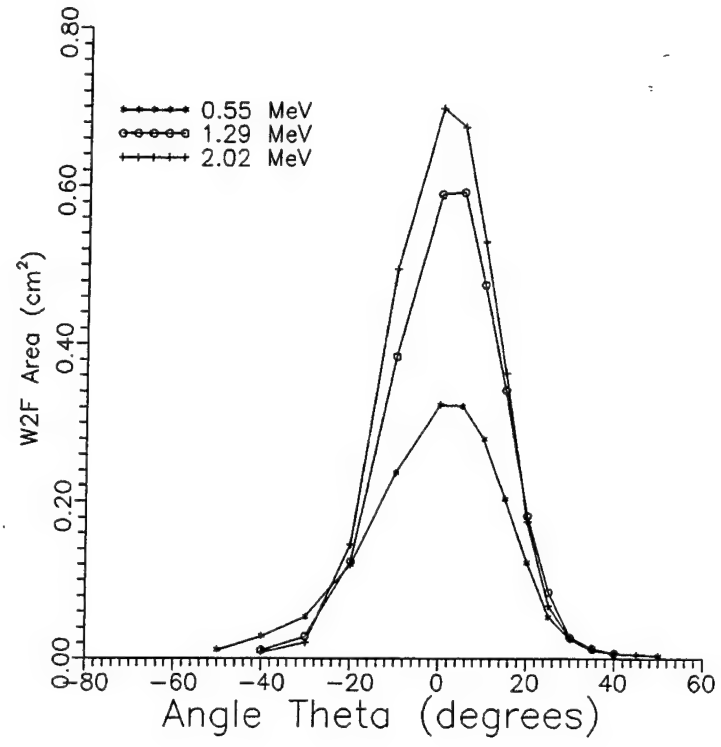

Figure 9. Measured Angular Response for Electrons of HEEF SN/2 SSDF/W2F.

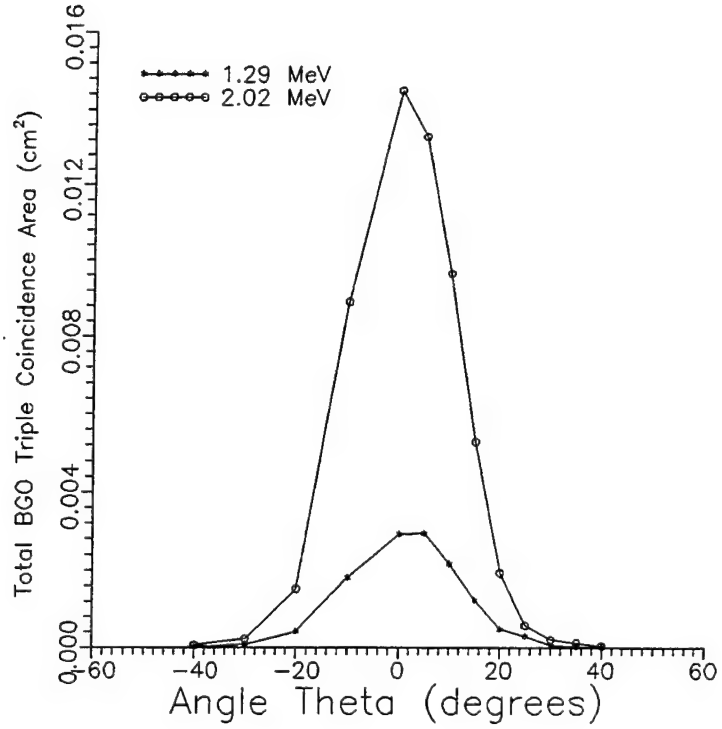

Figure 10. Measured Angular Response for Electrons of HEEF SN/2 BGO Triple Coincidence.

Table 18: Summary of HEEF SN/2 SSD Calibrated Geometric Factors and Energy Ranges for Electrons		
SSD Channel	G Factor (cm^2 sr)	Electron Energy Range
S1F	0.068	0.50 MeV < E_e < 1.35 MeV
"	0.036	E_e > 1.35 MeV
S2F	0.028	0.80 MeV < E_e < 1.35 MeV
"	0.014	E_e > 1.35 MeV
W1F	0.090	0.3 MeV < E_e < 1.0 MeV
"	0.15	1.0 MeV < E_e < 1.3 MeV
"	0.18	E_e > 1.3 MeV
W2F	0.14	0.3 MeV < E_e < 1.0 MeV
"	0.20	E_e > 1.0 MeV
S1B	0.0018	E_e > 0.85 MeV
S2B	0.0007	E_e > 1.05 MeV
W1B	0.0011	0.65 MeV < E_e < 0.95 MeV
"	0.0014 to 0.0094	E_e = 0.95 to 3.0 MeV, linear
W2B	0.0000 to 0.0032	E_e = 0.50 to 1.1 MeV, linear
"	0.0032 to 0.0108	E_e = 1.1 to 3.0 MeV, linear

Table 19: Best Fit Threshold Energies and Geometric Factors for Electrons of the SSD Channels		
SSD Channel	$E_{threshold}$ (MeV)	G_o (cm^2 sr)
S1F	0.48	0.060
S2F	0.74	0.020
W1F	0.30	0.120
W2F	0.30	0.15
S1B	0.83	0.0019
S2B	1.01	0.00075
W1B	0.72	0.0030
W2B	0.72	0.0040

3.3 Measured Response to Intense Beta Source Electron Fluxes

HEEF SN/2 was subjected to a large range of electron flux intensity using a 100 mCi Sr-Y-90 beta source. This beta source has an end point energy of 2.27 MeV with a broad peak near 0.8 MeV. The beta source was positioned on the FOV axis of HEEF at separations varying from 15 inches to 0.875 inches (source face to front of HEEF). The "effective" source-to-HEEF distance was about 1 inch greater since the HEEF collimation is the inner edge of the SSDF front collimator. The various SSDF, SSDB, and BGO PMT coincidence counts were measured for the beta source, and for the beta source plus a pulser into SSDF. The pulser was operated at 0.3 MeV, 1.0 MeV, 3.0 MeV and 10.0 MeV, at nominal frequencies of 1 kHz, 10 kHz and 100 kHz. The resulting compressed HEEF SSDF output count rates exceeded the range observed in-orbit by HEEF SN/1 on CRRES.

The beta source data were analyzed to obtain the count corrections for the S1FC, W1FC, S2FC and W2FC dead-time corrected count rates. The dead-time corrected count rates are calculated from

$$\begin{aligned} S1FC &= S1F/(1 - tau \times S1F) \\ S2FC &= S2F/(1 - tau \times S2F) \\ S1BC &= S1B/(1 - tau \times S1B) \\ S2BC &= S2B/(1 - tau \times S2B) \end{aligned} \qquad (3.8)$$

and

$$\begin{aligned} W1FC &= W1F \times DTFF1 \\ W2FC &= W2F \times DTFF2 \\ W1BC &= W1B \times DTFB1 \\ W2BC &= W2B \times DTFB2 \end{aligned} \qquad (3.9)$$

where

$$\begin{aligned} DTFF1 &= 1./[(1 - tau \times W1F) \times (1 - tau \times S1F)] \\ DTFF2 &= 1./[(1 - tau \times W2F) \times (1 - tau \times S2F)] \\ DTFB1 &= 1./[(1 - tau \times W1B) \times (1 - tau \times S1B)] \\ DTFB2 &= 1./[(1 - tau \times W2B) \times (1 - tau \times S2B)] \end{aligned} \qquad (3.10)$$

and tau = 1.1×10^{-6} s. The above equations are derived from the operation of the threshold and window circuitry of the SSD's, with the tau value being measured. The S1F and S2F outputs were also corrected for counter overflow, using the continuously recorded data from a slow in/out scan of the beta source. This allowed the clear observation of the several overflows and correlation with the source/HEEF separation.

The measured dead-time corrected count rates for the beta source are listed in Table 20. Table 21 lists the S + W sums and the average normalized SSDB response (average S + W multiplied by d_{eff}^2). This normalized average SSDB response is a good measure of the true beta source flux at the inner edge of the SSDF front collimator, since scattering in the Be foil and the SSDF produce an

electron intensity at SSDB that is directly proportional to that at SSDF. This is verified by the nearly constant value for the average SSDB response between about 10.0 and 2.75 inches for d_{eff}. The lower response at larger distances is the effect of energy loss by the electrons in the air, which eliminates some of the low energy electrons from the SSDB response. The rise at shorter distances comes from a slight offset in d_{eff} (a 0.14 inch decrease produces good agreement), and from small inaccuracies in the source position. Thus, the SSDB response is a good relative normalization for the true SSDF response, and can be used to calculate the paralyzation effects on the various SSDF output counts at high count rates.

The resulting effective responses for S1FC and S2FC relative to SSDB are listed in Table 22. The relative responses are then normalized to the four most distant points (15, 12, 9 and 7 inches source distance) where they are nearly constant, with (S1FC/SSDB)av = 19.801 and (S2FC/SSDB)av = 5.545, to give the extra correction factors S1FFX and S2FFX from

$$S1FFX(d) = 19.801 \; / \; S1FC(d) \tag{3.11}$$

and

$$S2FFX(d) = 5.545 \; / \; S2FC(d) \tag{3.12}$$

These are then used to calculate the "true" S1FCC and S2FCC count rates, which are also listed in Table 22. The completely corrected count rates are given by S1FCC = S1FC × S1FFX and S2FCC = S2FC × S2FFX. The S1FFX factors show a slow increase from 1.00 as S1FC increases above 100 kHz. The S2FFX factors first show a decrease resulting from pulse pile-up, and then an increase at the higher count rates. The CRRES in-orbit data from HEEF SN/1 give maximum values for S2FC of a bit above 100 kHz, so S2FC is mostly in the pulse pile-up region of correction. The maximum effect on S2FC is about 20% (20 kHz), and this is small compared with the S2FC + W2FC value of about 700 kHz at this maximum, so the corrections for S2FC can be neglected.

The dead-time corrections for the beta source + pulser data are more complex, since the pulser output is not random and thus does not affect itself until the pulse time separation equals the dead-time (this is at about 9 MHz). If the beta source count rates are taken as Bi and Bo for the input and output count rates, and the pulser count rates are taken as Pi and Po, then for a single threshold (S1F or S2F) the input count rates are related to the output count rates by

$$Bi = Bo \; / \; [1 - (Bo + Po) \times tau] \tag{3.13}$$

$$Pi = Po \; / \; (1 - Bo \times tau) \tag{3.14}$$

which give

$$Bi + Pi = \frac{Bo + Po - Pi^2 \times tau \times (1 - Bo \times tau)}{1 - (Bo + Po) \times tau} \qquad (3.15)$$

The above correction form is only required for the S1F and S2F calculations with the pulser at 1.0 and 3.0 MeV, since the 0.3 MeV pulser amplitude is below the S1F threshold value of 0.50 MeV and the S2F threshold of 0.80 MeV. For the 1.0 and 3.0 MeV pulser amplitude calculations, (Bo + Po) is the measured S1F or S2F output count rate, Pi was measured as 96 kHz, and Bo is estimated by using the beta-source-only output count rate measurements.

The correction factors for the beta source + pulser data are calculated from

$$S1FFX = S1FCC / S1FC \qquad (3.16)$$

for the 0.3 MeV pulser data, and from

$$S1FFX = (S1FCC + 96\ kHz) / S1FCP \qquad (3.17)$$

where S1FCP = Bi + Pi as calculated above for the 1.0 and 3.0 MeV pulser data.

The effective responses for S1FC for the pulser at 96 kHz and amplitudes of 0.3, 1.0 and 3.0 MeV are listed in Table 23 along with the extra correction factors S1FFX. The values of S1FC, S1F, and S1FCP listed are measured or calculated values, as described above. The beta source + pulser data have no normalization other than to the SSDB response. The main reason for performing the pulser tests was to verify that higher amplitude pulses (from protons, etc.) would not cause significant deviations from the beta-source measured correction factors. The results for the extra S1FC correction factor S1FFX are plotted in Figure 11, and show that the beta source + pulser data agree quite well with the beta source data. Thus, the S1FFX correction factors should be quite accurate for a wide range of pulse height spectra in SSDF, and the presence of proton fluxes should not change the corrections.

The 96 kHz pulser results for S2FC are listed in Table 24 and plotted in Figure 12. The 0.3 MeV pulser + beta source data agree well with the beta source only data. The 1 MeV pulser data show significant deviations, but this is because the pulser amplitude is near the S2F threshold of 0.80 MeV, and thus SSDF noise results in some of the pulses being below this threshold. The 1 MeV pulser data are thus not a true indication of the actual S2FC response. The 3 MeV pulser data are in better agreement with the beta source data, but are closer to 1.0 for S2FC below about 500 kHz. This is most likely because the pulser can not cause pile-up pulses with itself, so the pile-up effect observed with the beta source is reduced. Thus, the pulser tests show that the effects of a proton flux on the S2FC data from CRRES should not be significant.

The effective responses for W1FC and W2FC relative to SSDB are listed in Table 25. The responses have been normalized to the three furthest distance points (15, 12 and 9 inch source distances;

average of W1FC/SSDB(avg) = 42.14; average of W2FC/SSDB(avg) = 57.17) to calculate the extra correction factors W1FFX and W2FFX, and the true beta source count rates W1FCC and W2FCC. The measurements with the pulser at 96 kHz are summarized in Table 26 for W1FC and in Table 27 for W2FC. The pulser correction factors were calculated using the true W1FCC and W2FCC values from Table 25 with 96 kHz added for the 0.3 MeV pulser amplitude and 0 kHz for the 1.0 and 3.0 MeV pulser amplitudes. No additional normalization was used for these data at the low count rate end. Tables 25, 26 and 27 also list the measured, corrected count rate sums S1FC + W1FC and S2FC + W2FC. The extra correction factors W1FFX and W2FFX are plotted against these summed, dead-time corrected count rates in Figures 13 and 14.

Since the pulser output is not random, the pulser corrections are slightly incorrect, especially at the largest beta source distances. The precise method of correction for the W1F and W2F output count rates is rather complicated because both are "windows", with an upper threshold (S1F or S2F) in anti-coincidence with a lower threshold. The S1F and S2F correction method for the pulser data actually only provides a slight change from using the pure random pulse approach, so the W1F and W2F pulser + beta source data were analyzed by assuming that all pulses are random. No normalizations were made, since the W1FCC and W2FCC count rates from the beta source data and the measured pulser frequency of 96 kHz were used to calculate the correction factors.

The spread for the pulser data are mostly because there was no low count rate normalization as for the S1FFX data in Figure 11. The summed count rates S1FC + W1FC and S2FC + W2FC appear to give the best monotonic fit to the factors W1FFX and W2FFX. This method of obtaining the extra (paralyzation effect) correction factors W1FFX and W2FFX also provides a better form for the in-orbit data from HEEF SN/1.

The triple coincidence electron channel responses for HEEF SN/2 were also measured since the Sr-Y-90 beta source emits electrons up to 2.24 MeV. The measured responses for LL, L1 and L2 were corrected for dead-time effects by

$$LiC = Li \times DTFF2 \times DTFB2 \qquad (3.18)$$

where DTFF2 and DTFB2 are the SSDF and SSDB dead-time factors given earlier. The resulting count rates were summed and normalized to the SSDB response to derive an extra correction factor, BGOW2FFX, listed in Table 28. The normalization was to the measurements at the 15 inch source position, with no pulser. Table 28 also lists the sum S2FC + W2FC for the measurements, since W2F and W2B are used in the triple coincidence measurements for LL, L1 and L2 (see Table 8). The data in Table 28 are plotted in Figure 15, which shows that the 1 MeV and especially the 3 MeV pulser data deviate from the no-pulser and 0.3 MeV pulser data.

Table 20: HEEF SN/2 Measured SSD Dead-time Corrected Beta Source Count Rates

Source to HEEF Distance (inches)		Measured dead-time corrected channel count rates (kHz)							
Src/HEEF	Effective	S1FC	W1FC	S2FC	W2FC	S1BC	W1BC	S2BC	W2BC
15.0	16.0	20.47	43.97	5.62	59.17	0.41	0.64	0.11	0.93
12.0	13.0	35.52	75.19	9.72	102.01	0.66	1.09	0.18	1.57
9.0	10.0	64.56	134.63	18.00	184.20	1.23	2.02	0.35	2.90
7.0	8.0	103.58	206.73	30.41	285.8	1.99	3.33	0.56	4.75
5.0	6.0	179.74	318.14	58.52	445.3	3.57	5.97	1.00	8.54
4.0	5.0	262.4	391.5	95.38	548.6	5.48	9.22	1.57	13.15
3.0	4.0	386.3	439.4	167.8	599.6	9.11	15.16	2.56	21.77
2.25	3.25	494.4	445.7	253.2	593.0	13.41	22.49	3.77	32.24
1.75	2.75	585.4	437.5	348.8	571.8	19.19	32.17	5.43	46.21
1.25	2.25	686.9	410.7	489.2	534.4	31.00	51.76	8.81	74.61
1.0	2.0	724.2	394.9	553.3	513.7	38.69	64.83	11.05	93.45
0.875	1.875	747.6	381.7	598.0	497.3	46.37	77.36	13.34	111.77

Table 21: HEEF SN/2 Summed SSD Count Rates and Normalized SSDB Response

Source to HEEF Distance (inches)		Dead time corrected count rates (kHz)				Avg SSDB $(S+W)d_{eff}^2$ (kHz in^2)
Src/HEEF	Effective	S1FC+W1FC	S2FC+W2FC	S1BC+W1BC	S2BC+W2BC	
15.0	16.0	64.4	64.8	1.04	1.04	267.0
12.0	13.0	110.7	111.7	1.76	1.76	296.8
9.0	10.0	199.2	202.2	3.25	3.25	325.0
7.0	8.0	310.3	316.2	5.31	5.32	340.2
5.0	6.0	497.9	503.8	9.53	9.54	343.3
4.0	5.0	653.9	644.0	14.69	14.72	367.7
3.0	4.0	825.7	767.4	24.27	24.32	388.7
2.25	3.25	940.1	846.2	35.90	36.02	379.8
1.75	2.75	1023.0	920.6	51.35	51.63	389.4
1.25	2.25	1097.6	1023.6	82.76	83.42	420.6
1.0	2.0	1119.0	1067.0	103.52	104.50	416.0
0.875	1.875	1129.3	1095.3	123.73	125.11	437.4

Table 22: Relative Response and Extra Correction Factors for S1FC and S2FC - Beta Source Only

Source Distance (inches)	Measured S1FC/SSDB	Norm. Factor S1FFX	True S1FC = S1FCC (kHz)	Measured S2FC/SSDB	Norm. Factor S2FFX	True S2FC = S2FCC (kHz)
15.0	19.62	1.009	20.65	5.386	1.030	5.784
12.0	20.23	0.979	34.77	5.532	1.002	9.738
9.0	19.86	0.997	64.35	5.538	1.001	18.020
7.0	19.49	1.016	105.2	5.722	0.969	29.47
5.0	18.85	1.051	188.8	6.136	0.904	52.89
4.0	17.84	1.110	291.2	6.486	0.855	81.55
3.0	15.90	1.245	481.1	6.908	0.803	134.72
2.25	14.75	1.440	712.0	7.042	0.787	199.36
1.75	11.37	1.742	1019.6	6.773	0.819	285.5
1.25	8.27	2.395	1645.2	5.887	0.942	460.7
1.0	6.96	2.844	2059.	5.320	1.042	576.8
0.875	6.01	3.296	2464.	4.806	1.154	689.9

Table 23: Relative Response and Extra Correction Factors for S1FC - With Pulser

	Pulser 0.3 MeV / 96 kHz			Pulser 1.0 MeV / 96 kHz			Pulser 3.0 MeV / 96 kHz		
Source Distance (inches)	Measured S1F (kHz)	Calc. S1FC (kHz)	Calc. Factor S1FFX	Measured S1F (kHz)	Calc. S1FCP (kHz)	Calc. Factor S1FFX	Measured S1F (kHz)	Calc. S1FCP (kHz)	Calc. Factor S1FFX
15.0	20.83	21.32	0.969	111.0	115.1	1.013	110.4	114.3	1.020
12.0	35.22	35.64	0.949	121.8	129.4	1.011	122.1	129.8	1.008
9.0	62.06	66.60	0.966	141.3	156.2	1.027	141.9	157.0	1.022
7.0	95.35	106.52	0.988	165.9	191.8	1.049	166.6	192.8	1.044
5.0	153.30	184.39	1.024	208.8	260.0	1.095	209.3	261.0	1.091
4.0	206.4	267.1	1.090	248.9	331.8	1.167	249.3	332.7	1.164
3.0	273.4	390.9	1.231	299.8	436.7	1.321	300.1	437.3	1.320
2.25	321.6	497.7	1.430	337.2	525.6	1.537	337.3	525.9	1.536
1.75	356.9	587.7	1.735	365.5	600.8	1.857	365.7	602.3	1.852
1.25	391.5	687.7	2.392	395.0	688.1	2.530	394.5	686.8	2.535
1.0	403.2	724.7	2.842	405.1	720.4	2.992	404.8	719.6	2.995
0.875	410.4	748.1	3.293	411.9	743.1	3.445	411.5	741.7	3.451

The deviation is largest at low beta source count rates, and is most likely due to the SSDF pulse distortion due to the shorter pulser decay time. Since the triple coincidence timing is quite narrow (about 100 nsec total relative timing shift between two pulses), the SSDF pulse shape distortions from the fast pulser decay most likely affect the true electron triple coincidence efficiency by small shifts in the zero-cross pulse timing for electrons which are detected within a few microseconds after the pulser fires. This should be a larger percentage effect at low beta source count rates where the true electron-caused paralyzation effects are small. The corrections for the triple coincidence electron channels is thus best based on the no-pulser and the 0.3 MeV pulser data.

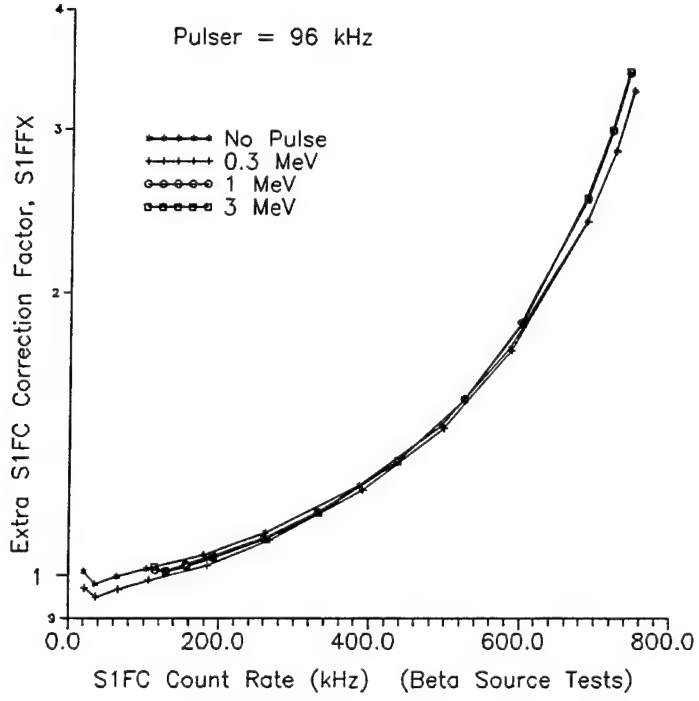

Figure 11. Measured Extra Correction Factors for S1FC for HEEF SN/2.

Table 24: Relative Response and Extra Correction Factors for S2FC - With Pulser

Source Distance (inches)	Pulser 0.3 MeV / 96 kHz Measured S2F (kHz)	Calc. S2FC (kHz)	Calc. Factor S2FFX	Pulser 1.0 MeV / 96 kHz Measured S2F (kHz)	Calc. S2FCP (kHz)	Calc. Factor S2FFX	Pulser 3.0 MeV / 96 kHz Measured S2F (kHz)	Calc. S2FCP (kHz)	Calc. Factor S2FFX
15.0	5.58	5.84	0.909	98.08	98.64	1.032	96.86	97.13	1.048
12.0	9.61	10.10	0.964	99.64	100.64	1.051	103.64	105.66	1.001
9.0	17.65	18.80	0.958	102.31	104.08	1.096	109.96	113.78	1.002
7.0	29.43	31.47	0.936	107.71	111.06	1.130	118.89	125.49	1.000
5.0	54.98	60.44	0.875	120.17	127.50	1.168	138.10	151.61	0.982
4.0	86.33	97.91	0.833	138.88	153.10	1.160	161.71	185.54	0.957
3.0	141.68	170.36	0.791	178.01	210.7	1.095	202.8	250.0	0.923
2.25	198.03	255.8	0.779	223.0	285.0	1.036	244.7	324.0	0.912
1.75	252.1	351.5	0.812	268.4	370.4	1.030	285.7	405.9	0.940
1.25	318.0	490.7	0.939	325.9	497.7	1.119	336.6	523.9	1.063
1.0	344.0	554.2	1.041	348.7	555.4	1.211	357.1	577.7	1.165
0.875	360.7	598.6	1.153	364.3	597.7	1.315	370.9	616.1	1.276

Table 25: Relative Response and Extra Correction Factors for W1FC and W2FC - Beta Source Only

Source Distance (inches)	Measured W1FC/SSDB	Norm. Factor W1FFX	True W1FC = W1FCC (kHz)	S1FC+W1FC (kHz)	Measured W2FC/SSDB	Norm. Factor W2FFX	True W2FC = W2FCC (kHz)	S2FC+W2FC (kHz)
15.0	42.16	1.000	43.95	64.4	56.73	1.008	59.63	64.8
12.0	42.82	0.984	74.00	110.7	58.09	0.984	100.39	111.7
9.0	41.43	1.017	136.94	199.2	56.68	1.009	185.79	202.2
7.0	38.90	1.083	223.95	310.3	53.78	1.063	303.8	316.2
5.0	33.36	1.263	401.9	497.9	46.69	1.224	545.2	503.8
4.0	26.62	1.583	619.7	653.9	37.31	1.533	840.7	644.0
3.0	18.084	2.330	1023.8	825.7	24.68	2.317	1389.0	767.4
2.25	12.396	3.40	1515.2	940.1	16.492	3.467	2056.	846.2
1.75	8.497	4.96	2170.	1023.0	11.105	5.148	2944.	920.6
1.25	4.943	8.53	3501.	1060.6	6.432	8.89	4750.	1023.6
1.0	3.797	11.10	4383.	1119.0	4.939	11.58	5946.	1067.0
0.875	3.068	13.74	5243.	1129.3	3.997	14.30	7113.	1095.3

Table 26: Relative Response and Extra Correction Factors for W1FC - With Pulser

Source Distance (inches)	Pulser 0.3 MeV / 96 kHz Measured W1FC (kHz)	S1FC +W1FC (kHz)	Extra Factor W1FFX	Pulser 1.0 MeV / 96 kHz Measured W1FC (kHz)	S1FC +W1FC (kHz)	Extra Factor W1FFX	Pulser 3.0 MeV / 96 kHz Measured W1FC (kHz)	S1FC +W1FC (kHz)	Extra Factor W1FFX
15.0	146.5	167.8	0.955	40.9	167.3	1.075	41.0	166.6	1.071
12.0	175.2	211.8	0.970	69.9	210.5	1.059	63.8	204.9	1.160
9.0	240.7	307.3	0.968	124.1	291.5	1.103	112.9	281.1	1.213
7.0	284.9	391.4	1.123	189.4	392.4	1.182	171.2	375.1	1.308
5.0	368.3	552.7	1.352	290.8	561.8	1.382	259.8	531.8	1.547
4.0	418.3	685.4	1.711	362.8	705.5	1.708	362.8	705.5	1.927
3.0	446.0	836.9	2.511	415.6	862.9	2.463	367.4	815.3	2.787
2.25	446.3	944.0	3.610	432.1	968.2	3.507	382.5	918.8	3.961
1.75	436.6	1024.3	5.19	428.5	1039.6	5.06	381.9	993.8	5.68
1.25	410.2	1097.9	8.77	407.4	1105.7	8.59	369.9	1066.9	9.47
1.0	394.6	1119.3	11.35	391.7	1122.3	11.19	361.2	1091.0	12.13
0.875	381.5	1129.6	13.99	379.7	1133.0	13.81	353.4	1105.3	14.84

Table 27: Relative Response and Extra Correction Factors for W2FC - With Pulser

Source Distance (inches)	Pulser 0.3 MeV / 96 kHz Measured W2FC (kHz)	S2FC +W2FC (kHz)	Extra Factor W2FFX	Pulser 1.0 MeV / 96 kHz Measured W2FC (kHz)	S2FC +W2FC (kHz)	Extra Factor W2FFX	Pulser 3.0 MeV / 96 kHz Measured W2FC (kHz)	S2FC +W2FC (kHz)	Extra Factor W2FFX
15.0	163.8	169.6	0.950	55.0	164.9	1.084	55.5	163.9	1.074
12.0	205.1	215.2	0.958	94.6	206.5	1.062	86.4	203.4	1.162
9.0	281.2	300.0	1.002	169.4	284.7	1.097	153.4	278.5	1.211
7.0	369.6	401.1	1.082	260.4	382.6	1.167	233.5	370.3	1.302
5.0	499.9	560.3	1.283	403.8	542.3	1.350	353.2	516.0	1.544
4.0	576.2	674.1	1.626	503.8	667.7	1.669	434.0	630.7	1.937
3.0	606.4	776.8	2.449	567.4	788.7	2.448	485.5	746.5	2.861
2.25	593.9	849.7	3.623	573.3	868.9	3.586	496.3	831.1	4.142
1.75	570.5	922.0	5.33	559.8	940.6	5.26	494.5	911.1	5.95
1.25	533.5	1024.2	9.08	529.2	1037.1	8.98	479.7	1014.1	9.90
1.0	513.6	1067.9	11.76	509.3	1074.9	11.67	468.0	1056.0	12.71
0.875	496.2	1094.8	14.53	493.6	1101.5	14.41	459.2	1085.6	15.49

Table 28: Relative Response and Extra Correction Factors for LL + L1 + L2

Source Distance (inches)	Beta Source/No Pulser: Measured LL+L1+L2 (Hz)	Beta Source/No Pulser: 1000 × LL+L1+L2 SSDB(avg)	Beta Source/No Pulser: S2FC +W2FC (kHz)	Beta Source/No Pulser: Extra Factor BGOW2FFX	Pulser 0.3 MeV/96 kHz: Measured LL+L1+L2 (Hz)	Pulser 0.3 MeV/96 kHz: 1000 × LL+L1+L2 SSDB(avg)	Pulser 0.3 MeV/96 kHz: S2FC +W2FC (kHz)	Pulser 0.3 MeV/96 kHz: Extra Factor BGOW2FFX
15.0	150.5	144.30	64.8	0.994	139.8	134.04	169.6	1.070
12.0	250.4	142.60	111.7	1.006	223.4	127.22	215.2	1.128
9.0	411.5	126.62	202.2	1.133	383.9	118.12	300.0	1.214
7.0	585.3	110.12	316.2	1.303	530.1	99.74	401.1	1.438
5.0	723.5	75.86	503.8	1.891	660.1	69.21	560.3	2.073
4.0	741.8	50.44	644.0	2.844	685.6	46.62	674.1	3.077
3.0	638.6	26.28	767.4	5.46	609.0	25.07	776.8	5.72
2.25	614.1	17.079	846.2	8.40	627.0	17.438	849.7	8.23
1.75	723.9	14.058	920.6	10.20	745.7	14.482	922.0	9.91
1.25	968.3	11.654	1023.6	12.31	919.7	11.069	1024.2	12.96
1.0	1090.5	10.485	1067.0	13.68	1053.3	10.127	1067.9	14.17
0.875	1200.6	9.649	1095.3	14.87	1210.3	9.727	1094.8	14.75

Source Distance (inches)	Pulser 1.0 MeV/96 kHz: Measured LL+L1+L2 (Hz)	Pulser 1.0 MeV/96 kHz: 1000 × LL+L1+L2 SSDB(avg)	Pulser 1.0 MeV/96 kHz: S2FC +W2FC (kHz)	Pulser 1.0 MeV/96 kHz: Extra Factor BGOW2FFX	Pulser 3.0 MeV/96 kHz: Measured LL+L1+L2 (Hz)	Pulser 3.0 MeV/96 kHz: 1000 × LL+L1+L2 SSDB(avg)	Pulser 3.0 MeV/96 kHz: S2FC +W2FC (kHz)	Pulser 3.0 MeV/96 kHz: Extra Factor BGOW2FFX
15.0	122.4	117.35	164.9	1.222	117.2	112.37	163.9	1.277
12.0	190.2	108.31	206.5	1.324	118.6	67.54	203.4	2.124
9.0	316.5	97.38	284.7	1.473	201.3	61.94	278.5	2.316
7.0	440.2	82.82	382.6	1.732	283.2	53.28	370.3	2.692
5.0	550.4	57.71	542.3	2.486	416.9	43.71	516.0	3.282
4.0	589.1	40.06	667.7	3.581	469.8	31.95	630.7	4.490
3.0	541.9	22.30	788.7	6.43	478.9	19.711	746.5	7.28
2.25	579.1	16.106	868.9	8.91	531.6	14.785	831.1	9.70
1.75	700.6	13.606	940.6	10.54	626.5	12.167	911.1	11.79
1.25	931.7	11.213	1037.1	12.79	849.4	10.223	1014.1	14.03
1.0	1052.4	10.119	1074.9	14.18	991.7	9.535	1056.0	15.04
0.875	1218.2	9.791	1101.5	14.65	1065.1	8.560	1085.6	16.76

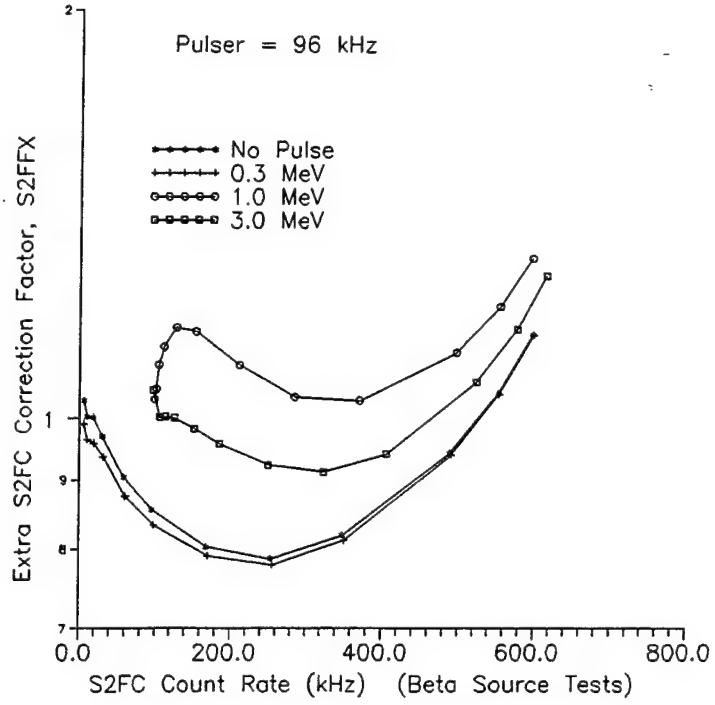

Figure 12. Measured Extra Correction Factors for S2FC for HEEF SN/2.

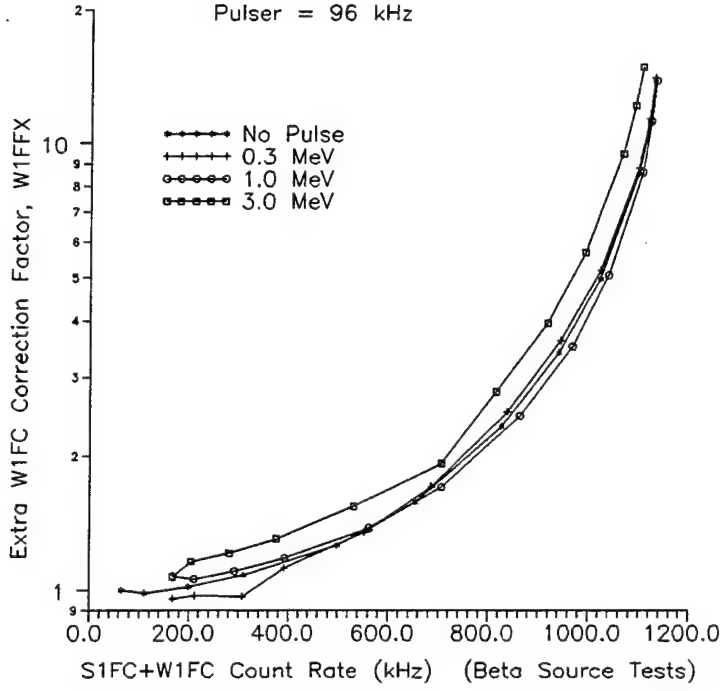

Figure 13. Measured Extra Correction Factors for W1FC for HEEF SN/2.

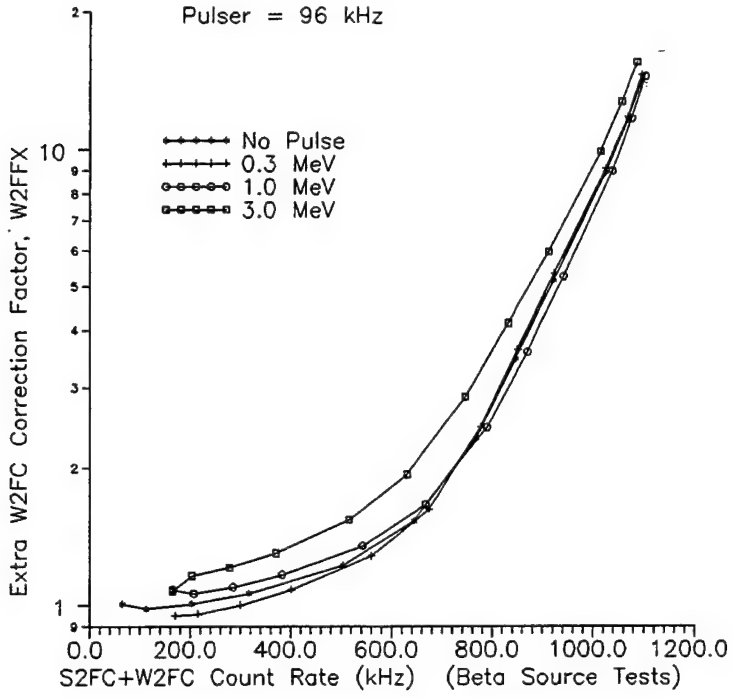

Figure 14. Measured Extra Correction Factors for W2FC for HEEF SN/2.

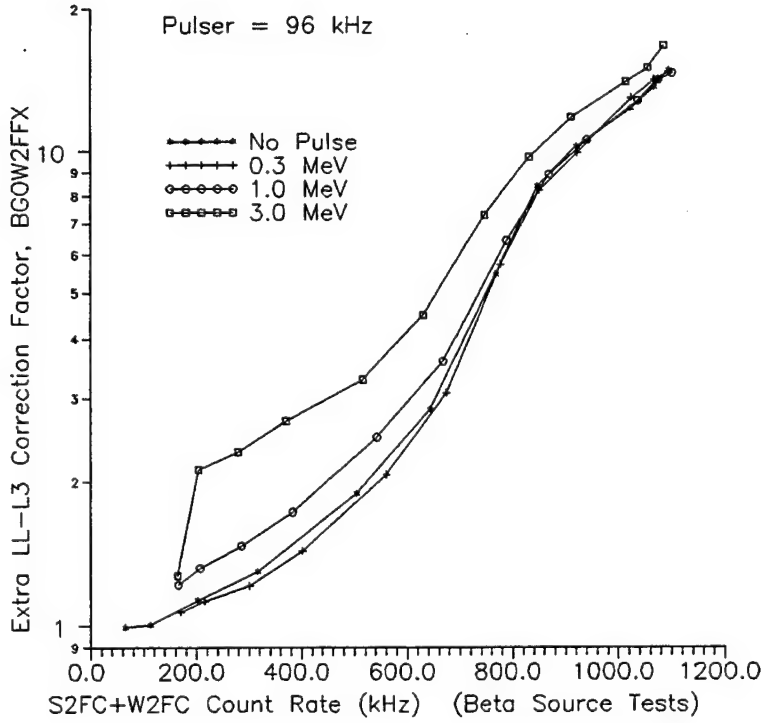

Figure 15. Measured Extra Correction Factors for LL to L3 Channels for HEEF SN/2.

3.4 Data Analysis Procedures

The HEEF SN/1 on CRRES provides a complete set of counts every 0.512 second. The output counts, in compressed form, are:

S2F, S1F, W2F, W1F, S2B, S1B, W2B, W1B - from the SSD's
LL, L1, L2, L3, L4, L5, L6, L7, L8, L9, L10C - BGO Coincidence
BGO, L10S - total BGO counts above LL, and above L10
LS - anti-coincidence scintillator total counts

The above counts must first be decompressed to obtain the corresponding input count (range), and then converted to a count rate by dividing by 0.512 s. The HEEF data from CRRES have some periods of intense electron fluxes when the S1F and S2F counters overflow. Under these conditions the S1F and S2F counts must first be corrected for the overflow by adding an appropriate multiple of 32768 to the decompressed count. The number of overflows must be tracked from a time of low count rates when there are no overflows by counting up or down by one whenever successive counts change by more than half of the overflow value (32768/2 = 16384). Accuracy can be checked by verifying that the overflow count returns to 0 when the flux returns to low values.

The output HEEF count rates (or averages, if several counts are added) must be corrected for deadtime effects. The non-paralyzation deadtime corrections are made by first calculating four dead-time correction factors from the measured (output) count rates (the notation W1F, W2F, etc. is now used to represent the measured count rates in counts/second):

$$\begin{aligned} DTFF1 &= 1./[(1 - tau \times W1F)\times(1 - tau \times S1F)] \\ DTFF2 &= 1./[(1 - tau \times W2F)\times(1 - tau \times S2F)] \\ DTFB1 &= 1./[(1 - tau \times W1B)\times(1 - tau \times S1B)] \\ DTFB2 &= 1./[(1 - tau \times W2B)\times(1 - tau \times S2B)] \end{aligned} \qquad (3.19)$$

where tau = 1.1×10^{-6} s is the measured dead-time. Next the dead-time corrected SSD single threshold count rates are calculated from

$$\begin{aligned} S1FC &= S1F/(1 - tau \times S1F) \\ S2FC &= S2F/(1 - tau \times S2F) \\ S1BC &= S1B/(1 - tau \times S1B) \\ S2BC &= S2B/(1 - tau \times S2B) \end{aligned} \qquad (3.20)$$

and the dead-time corrected SSD window count rates are calculated from

$$\begin{aligned} W1FC &= W1F \times DTFF1 \\ W2FC &= W2F \times DTFF2 \\ W1BC &= W1B \times DTFB1 \\ W2BC &= W2B \times DTFB2 \end{aligned} \qquad (3.21)$$

The dead-time corrected total BGO and anti-coincidence scintillator free count rates are calculated from

$$BGOC = BGO/(1 - tau \times BGO) \quad (3.22)$$

$$L10SC = L10S/(1 - tau \times L10S) \quad (3.23)$$

$$LSC = LS/(1 - tau \times LS) \quad (3.24)$$

The above are needed for paralyzation effect corrections, and for accidental coincidence count rate calculations.

If the SSDF count rates are very high, then the triple coincidence BGO count rates must be corrected for accidental coincidences. The total output count rate from accidental coincidences is given by

$$C1ACC = W1F \times W1B \times BGO \times taur^2 \quad (3.25)$$

and

$$C2ACC = W2F \times W2B \times BGO \times taur^2 \quad (3.26)$$

where taur = 1.0×10^{-7} s is the measured resolving time of the coincidence circuitry. The value of C2ACC is for the LL - L3 channels, while C1ACC is for the L4 - L9 channels, in the triple coincidence mode of operation.

The dead-time and accidental coincidence corrected BGO coincidence count rates are calculated from

$$LiC = (Li - C2ACC \times Lifrac) \times DTFF2 \times DTFB2 \quad (3.27)$$

for LL, L1, L2 and L3, and

$$LiC = (Li - C1ACC \times Lifrac) \times DTFF1 \times DTFB1 \quad (3.28)$$

for L4, L5, L6, L7, L8, and L9. The value of Lifrac is the fraction of output counts which are in channel Li, and is given by

$$Lifrac = Li/(LL + L1 + \ldots + L8 + L9) \quad (3.29).$$

Note that the above calculations use the measured output count rates from telemetry. For the L10C channel the accidental corrections are calculated using the measured L10S count rate from

$$L10CC = (L10C - W1F \times W1B \times L10S \times taur^2) \times DTFF1 \times DTFB1 \quad (3.30).$$

The result of the above is a set of dead-time corrected count rates, which are then corrected for paralyzation effects, if necessary, and used for particle flux calculation.

The paralyzation effect corrections required at very high SSDF count rates are as follows:

(1) If S1FC > 100 kHz, then a paralyzation correction factor is required to give

$$S1FCC = S1FC \times S1FFX \quad (3.31)$$

S1FFX is obtained from Table 29 using S1FC for interpolation. Table 29 is averaged over the beta source and beta source + pulser data of Tables 22 and 23.

(2) If S1FC + W1FC > 200 kHz, then a paralyzation correction factor is required to give

$$W1FCC = W1FC \times W1FFX \quad (3.32)$$

W1FFX is obtained from Table 30 using S1FC + W1FC for interpolation. The data in Table 30 are averages over the beta source and beta source + pulser data for HEEF SN/2 in Tables 25 and 26, adjusted slightly to give better agreement between S1FCC + W1FCC and S2FCC + W2FCC for in-orbit data from HEEF SN/1 on CRRES. Table 30 shows two sets of factors: the first are the measured averaged data from HEEF SN/2; the second are the adjusted factors for HEEF SN/1 in CRRES.

(3) If S2FC + W2FC > 200 kHz, then a paralyzation correction factor is required to give

$$W2FCC = W2FC \times W2FFX \quad (3.33)$$

W2FFX is obtained from Table 31 using S2FC + W2FC for interpolation. The data in Table 31 are averages over the beta source and beta source + pulser data for HEEF SN/2 in Tables 25 and 27. The same factors are used for HEEF SN/2 in CRRES.

(4) If S2FC + W2FC is greater than 65 kHz, then a paralyzation correction factor is required to give

$$LiCC = LiC \times BGOW2FFX \quad (3.34)$$

where LiC is LLC, L1C, L2C or L3C. BGOW2FFX is obtained from Table 32 using S2FC + W2FC for interpolation. The data in Table 32 is an average of the beta source and beta source + 0.3 MeV pulser data in Table 28.

(5) If S1FC + W1FC is greater than 81 kHz, then a paralyzation correction factor is required to give

$$LiCC = LiC \times BGOW1FFX \quad (3.35)$$

where LiC is L4C, L5C, L6C, L7C, L8C, L9C or L10CC. BGOW1FFX is obtained from Table 32 using S1FC + W1FC for interpolation. The S1FC + W1FC values in Table 32 are based on the beta source LL + L1 + L2 data, but corrected to provide better spectral shape continuity from the L3 to L4 points for the CRRES data. The CRRES HEEF spectral shapes show the least L3 - L4 discontinuity when (S1FC + W1FC) = (S2FC + W2FC)/0.80 in Table 32, as shown by the listed count rate values.

Table 29: Paralyzation Correction Factor S1FFX	
Measured S1FC (kHz)	Extra S1FC Correction Factor S1FFX
100.	1.00
190.	1.05
265.	1.10
390.	1.24
500.	1.45
590.	1.75
690.	2.40
725.	2.85
750.	3.3
Results are from beta source + pulser (96 kHz; 0.3, 1.0, and 3.0 MeV) tests on HEEF SN/2.	

Table 30: Paralyzation Correction Factor W1FFX		
Measured S1FC+W1FC (kHz)	HEEF SN/2 Measured Extra W1FC Correction Factor W1FFX(SN/2)	HEEF SN/1 Adjusted Extra W1FC Correction Factor W1FFX(SN/1)
200.	1.00	1.00
300.	1.05	1.09
400.	1.15	1.17
500.	1.25	1.32
550.	1.35	1.40
650.	1.55	1.68
700.	1.70	1.88
840.	2.4	2.23
950.	3.5	2.8
1025.	5.0	3.9
1100.	8.5	6.4
1120.	11.2	8.4
1130.	13.8	10.4
W1FFX(SN/2) results are from beta source + pulser (96 kHz; 0.3 and 1.0 MeV) tests on HEEF SN/2. W1FFX(SN/1) are the W1FFX(SN/2) data adjusted to provide better agreement between S1FCC+W1FCC and S2FCC+W2FCC for in-orbit CRRES data.		

Table 31: Paralyzation Correction Factor W2FFX	
Measured S2FC+W2FC (kHz)	Extra W2FC Correction Factor W2FFX
200.	1.00
300.	1.05
400.	1.12
500.	1.25
550.	1.32
650.	1.60
780.	2.4
850.	3.6
925.	5.2
1025.	9.0
1070.	11.7
1100.	14.4
Results are from beta source + pulser (96 kHz; 0.3 and 1.0 MeV) tests on HEEF SN/2.	

Particle fluxes are calculated from the fully corrected count rates using the appropriate geometric factors. For the SSDs the geometric factors are shown in Figure 8 and summarized in Tables 18 and 19. If no protons are present, integral electron fluxes can be calculated from W1FCC, W2FCC, S1FCC, W1BC, W2BC, S2FC (may have pile-up contamination), S1BC and S2BC. Reasonably accurate integral fluxes J_e can be calculated using the low energy G_{oi} factors (cm^2 sr) from Table 19 to give

$$J_e(E_{ei}) = WiFCC/G_{oi} \qquad (3.36)$$

where E_{ei} is the effective threshold energy for channel i. These integral electron fluxes will be most accurate for spectra which decrease at higher energies, although the Table 19 fits are reasonably accurate for power law exponents in the range of 0 to 8 ($E^{-\gamma}$ differential spectrum shape). If desired, slightly more precise spectral information can be obtained by using more elaborate fitting procedures with the complete energy variation of the geometric factors in Figure 8 and Tables 16 and 17.

Differential electron fluxes can be calculated from the fully corrected BGO coincidence count rates, LLCC, L1CC, --- L9CC (L10CC for integral fluxes). The differential electron spectrum is calculated from

$$dJ(E_i)/dE = LiCC/G_E(i) \quad el/(cm^2\ s\ sr\ keV) \qquad (3.37)$$

where $G_E(i)$ is the energy-geometric factor of channel i in (cm^2 sr

Table 32: Paralyzation Correction Factors BGOW2FFX and BGOW1FFX			
Measured S2FC+W2FC for BGOW2FFX (kHz)	LL-L3 BGOW2FFX	L4-L10C BGOW1FFX	S1FC+W1FC for BGOW1FFX (kHz)
	Extra Correction Factor		
65.	1.00		81.
110.	1.01		138.
170.	1.07		213.
210.	1.13		263.
310.	1.26		388.
400.	1.44		500.
530.	2.0		663.
660.	3.0		825.
780.	5.9		975.
850.	8.4		1063.
930.	10.2		1163.
1025.	12.7		1281.
1070.	14.0		1338.
1095.	14.7		1369.

BGOW2FFX results are from beta source, and beta source + 0.3 MeV pulser data from HEEF SN/2. The BGOW1FFX factors have been adjusted to provide better agreement for in-orbit data from HEEF SN/1 in CRRES, and are obtained from

(S1FC + W1FC) = (S2FC + W2FC)/0.80

keV) (for L10CC it is the integral geometric factor in (cm^2 sr)). The values of $G_E(i)$ depend on both the HEEF HV step setting for PMT gain, and on the temperature for the BGO crystal gain and pulse timing. The calculation of the $G_E(i)$ values is described in References 4 and 5, which includes fits to the temperature measurements made with HEEF SN/2. For HEEF SN/1 in CRRES, the fits of Reference 5 are best using a timing offset t_r = 0 ns and a maximum time difference d_m = 50 ns. Using these values, the average energy and energy-geometric factors for HEEF SN/1 on CRRES at HV 128 (the normal operating HV step) for a number of temperatures are listed in Tables 33 to 36. The listed values of $G_E(i) = G \times \Delta E$ are taken directly from Reference 5 method calculations, except that the value for LL is multiplied by 3. The HEEF SN/2 calibration data in Table 15 and Figure 7 are better fit with this factor increase since the LL channel response has a significant high energy "tail". The values for L10C are the electron threshold energy and the effective geometric factor in (cm^2 sr). Note that the L10C channel also responds to high energy protons (>270 MeV), and thus is not a clean electron channel. HEEF SN/1 operated in the temperature range of 0°C to -10°C for most of the CRRES lifetime. A computer program performing the Reference 5 calculations has been provided to PL to generate the responses for

different temperatures and HV steps.

Table 33: Average Channel Energies and Energy-Geometric Factors for HEEF SN/1 at 25°C		
Channel	Average E_e (MeV)[1]	G × ΔE (cm^2 sr keV)
LL	1.34	0.465[2]
L1	1.74	0.524
L2	2.26	0.999
L3	2.72	1.272
L4	3.22	1.704
L5	3.74	1.946
L6	4.40	4.68
L7	5.39	5.85
L8	6.76	11.47
L9	8.77	12.27
L10C	>10.00	6.13[3]

[1] For LL to L9 the E_e values are for a n = 6 spectrum ($dJ/dE = K E^{-6}$).
[2] For LL the value of G × ΔE has been multiplied by 3 to give a better fit to the SN/2 calibration data (see text).
[3] For L10C E_e is the threshold in MeV and G in (cm^2 sr) is given.

Table 34: Average Channel Energies and Energy-Geometric Factors for HEEF SN/1 at 10°C		
Channel	Average E_e (MeV)[1]	G × ΔE (cm^2 sr keV)
LL	1.27	0.200[2]
L1	1.61	0.265
L2	2.07	0.538
L3	2.49	0.709
L4	2.95	0.980
L5	3.42	1.150
L6	4.03	2.86
L7	4.93	3.71
L8	6.18	7.50
L9	8.03	8.30
L10C	>9.15	4.53[3]

[1] For LL to L9 the E_e values are for a n = 6 spectrum ($dJ/dE = K E^{-6}$).
[2] For LL the value of G × ΔE has been multiplied by 3 to give a better fit to the SN/2 calibration data (see text).
[3] For L10C E_e is the threshold in MeV and G in (cm^2 sr) is given.

Table 35: Average Channel Energies and Energy-Geometric Factors for HEEF SN/1 at 0°C		
Channel	Average E_e (MeV)[1]	G × ΔE (cm^2 sr keV)
LL	1.23	0.0810[2]
L1	1.52	0.1151
L2	1.96	0.230
L3	2.36	0.295
L4	2.79	0.395
L5	3.23	0.448
L6	3.80	1.065
L7	4.65	1.302
L8	5.83	2.41
L9	7.57	2.40
L10C	>8.65	1.385[3]

[1] For LL to L9 the E_e values are for a n = 6 spectrum ($dJ/dE = K E^{-6}$).
[2] For LL the value of G × ΔE has been multiplied by 3 to give a better fit to the SN/2 calibration data (see text).
[3] For L10C E_e is the threshold in MeV and G in (cm^2 sr) is given.

Table 36: Average Channel Energies and Energy-Geometric Factors for HEEF SN/1 at -10°C		
Channel	Average E_e (MeV)[1]	G × ΔE (cm^2 sr keV)
LL	1.19	0.0261[2]
L1	1.45	0.0381
L2	1.85	0.0690
L3	2.23	0.0802
L4	2.63	0.0957
L5	3.06	0.0975
L6	3.59	0.1981
L7	4.39	0.1992
L8	5.48	0.278
L9	7.13	0.1949
L10C	>8.21	0.1188[3]

[1] For LL to L9 the E_e values are for a n = 6 spectrum ($dJ/dE = K E^{-6}$).
[2] For LL the value of G × ΔE has been multiplied by 3 to give a better fit to the SN/2 calibration data (see text).
[3] For L10C E_e is the threshold in MeV and G in (cm^2 sr) is given.

4. Analysis of CRRES Data

4.1 Measured HEEF Electron Spectra

CRRES provided HEEF data for more than 1000 orbits, covering a range of magnetospheric activity levels. Processing of the bulk of the HEEF data from CRRES is done at PL. To illustrate the operation of HEEF, several fully corrected HEEF electron spectra are presented and discussed in this section. The results demonstrate the expected accuracy of the reduced electron fluxes.

HEEF normally provides a ten-point differential electron spectrum from the triple coincidence BGO spectrum, but in the absence of significant proton fluxes the SSD singles channels also provide several lower energy integral channels. The SSD integral electron channel responses are summarized in Table 19. For electron spectra not contaminated by proton fluxes, it is possible to use the S1F-S2F and S1B-S2B integral flux differences to provide two differential channels centered at 0.61 MeV (S1F-S2F) and 0.92 MeV (S1B-S2B). In the absence of proton contamination the S2B channel provides an integral flux above 1.01 MeV electron energy, J(>1.01,S2B). By integrating the 10-channel BGO electron spectrum from 1.01 MeV, it is possible to generate an integral electron flux, J(>1.01,BGO), which can then be compared with J(>1.01,S2B). Since the S2B channel usually has small deadtime corrections, this allows a good cross check between the SSDB electron response and the BGO electron response.

HEEF spectra from a time when there is good agreement between the BGO (triple coincidence) electron spectrum and the SSD-derived spectrum are shown in Figures 16 and 17, taken from high L values of orbits 75 (L = 5.36) and 76 (L = 6.75). All of the HEEF electron spectra plots show the electron flux in el/(cm^2 s sr MeV) for the differential fluxes (DJ/DE) and el/(cm^2 s sr) for the integral fluxes (JEint, or J(>E)). For these spectra there is a significant high energy electron flux with only a low (cosmic ray background) proton flux. Thus, the SSD channels provide good electron spectra. Note that the two differential channels from SSDF and SSDB fit very well with the higher energy BGO electron spectrum. The BGO differential spectrum and the SSD integral spectrum have both been fit with a power law shape. The ratios of the integral electron fluxes, J(>1.01,BGO)/J(>1.01,S2B), are 1.08 for orbit 75 (Figure 16) and 0.93 for orbit 76 (Figure 17), which is excellent agreement. The HEEF sensor temperature was about -4°C for these two spectra, and the corresponding geometric factors have been used (values are between those listed in Tables 35 and 36).

Electron spectra for more intense fluxes are shown in Figures 18 (orbit 20, L = 3.47), 19 (orbit 12, L = 3.17) and 20 (orbit 76, L = 3.68). The S1B-S2B SSDB differential spectrum point at 0.92 MeV is still in reasonable agreement with the BGO differential spectrum, but the S1F-S2F SSDF differential spectrum point at 0.61 MeV is questionable, especially in Figure 20. For these three spectra the total SSDF count rate is about 1.2 MHz, 1.5 MHz, and 1.4 MHz, so the SSDF deadtime correction factors are large. The

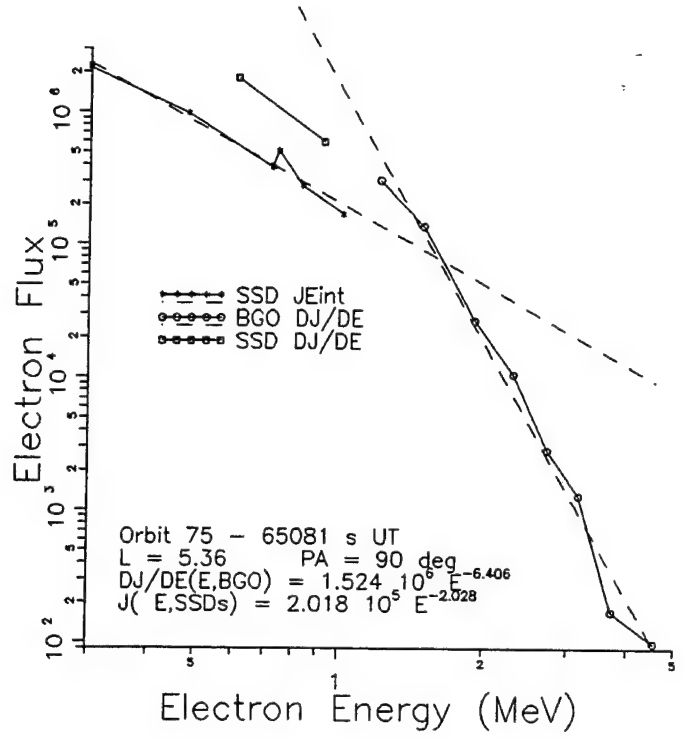

Figure 16. HEEF Electron Spectrum for Orbit 75, L = 5.36.

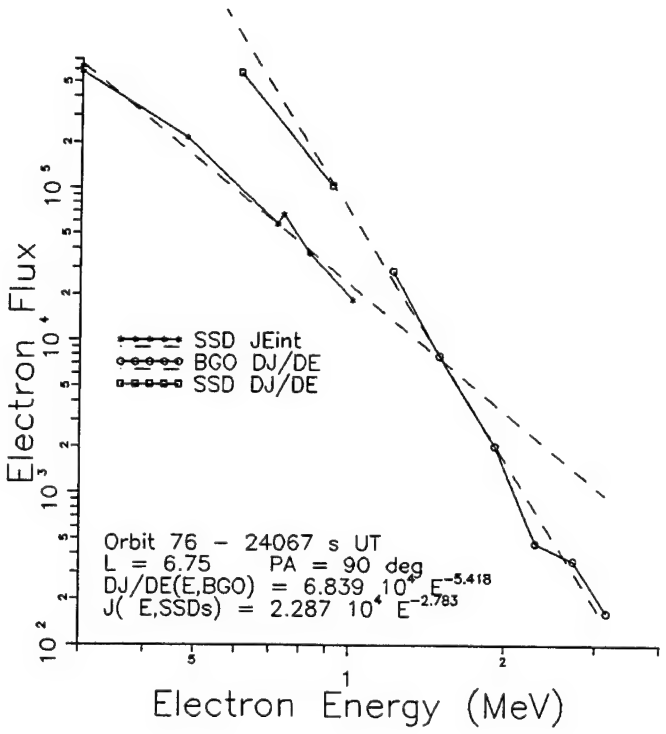

Figure 17. HEEF Electron Spectrum for Orbit 76, L = 6.75.

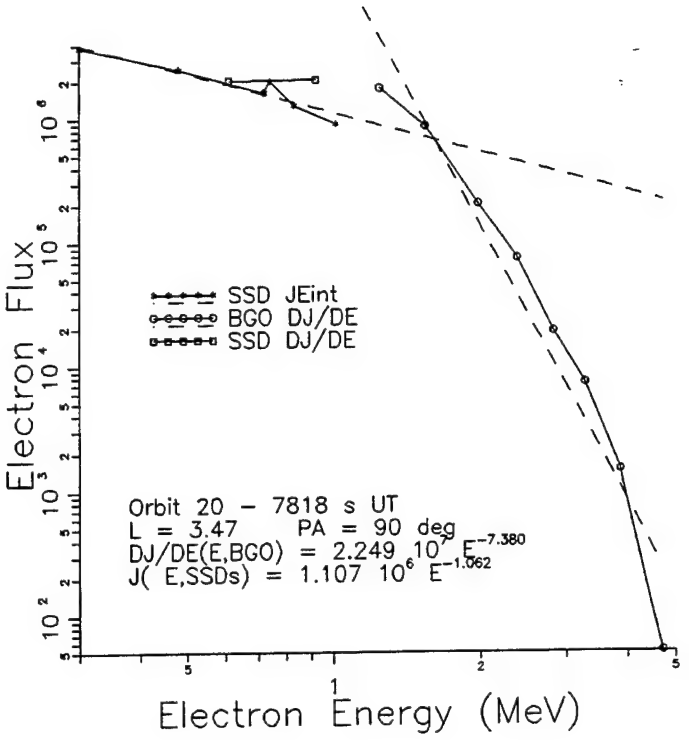

Figure 18. HEEF Electron Spectrum for Orbit 20, L = 3.7.

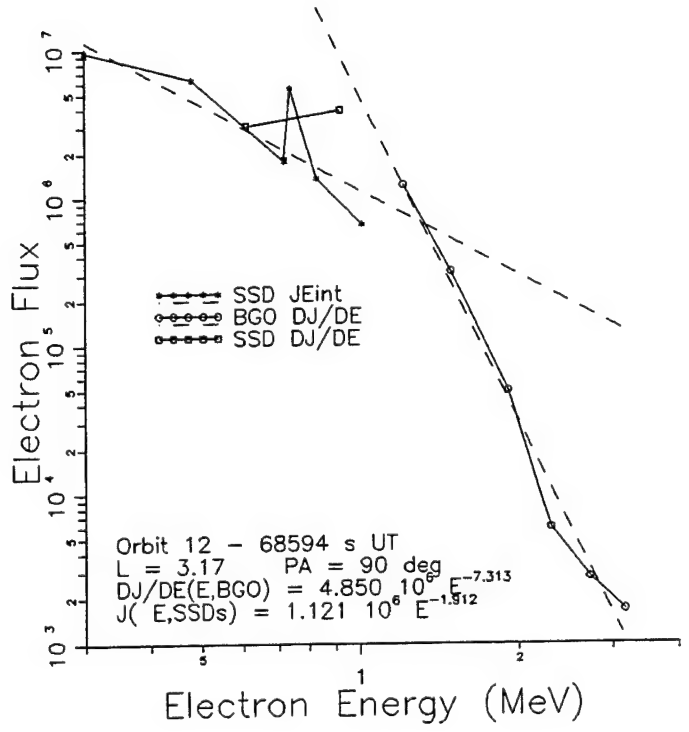

Figure 19. HEEF Electron Spectrum for Orbit 12, L = 3.17.

integral electron flux ratios J(>1.01,BGO)/J(>1.01,S2B) are 1.35 for orbit 20 (Figure 18), 1.08 for orbit 12 (Figure 19), and 1.48 for orbit 76 (Figure 20), which is reasonably good agreement. The HEEF sensor temperatures used to calculate the geometric factors were -4°C for orbits 12 and 76, and +2°C for orbit 20.

HEEF electron spectra for orbit 61, L = 3.85, orbit 250, L = 6.62, and orbit 250, L = 4.64 are shown in Figures 21, 22 and 23. These three higher L spectra show good agreement between the BGO and SSD electron spectra. A HEEF electron spectrum for orbit 250, L = 3.64, is shown in Figure 24. Here, the agreement between the BGO and SSD spectra is not as good, and is likely due to the rather flat electron spectral shape below about 1 MeV, with a steep ($E^{-5.5}$) spectral drop above 1 MeV. For electron spectra with this type of shape, the SSD channel responses are not accurately approximated by a fixed energy threshold, and thus the SSD differential electron spectrum points deviate significantly from the BGO measurements. The integral electron flux ratios J(>1.01,BGO)/J(>1.01,S2B) are 1.33 for orbit 61 (Figure 21), 1.39 for orbit 250, L = 6.62 (Figure 22), 1.61 for orbit 250, L = 4.64 (Figure 23), and 1.69 for orbit 250, L = 3.64 (Figure 24), which is reasonable agreement. Thus the integral electron spectra from the BGO and SSDB (S2B) are still in reasonable agreement for Figure 24, even though the differential spectra deviate by more than a factor of 10. The BGO data were processed using a HEEF sensor temperature of -4°C for orbit 61, and -10°C for orbit 250.

HEEF electron spectra for very intense electron fluxes are calculated using some very large correction factors (see Section 3.4), and this introduces some larger uncertainties in the absolute spectral intensities. This is particularly true for the SSDF channels, which can have very large deadtime corrections. The effect is illustrated by several spectra from orbits 600 and 602, shown in Figures 25 to 29. Figure 25 shows a spectrum from orbit 600, L = 3.51, where the SSD differential spectrum points are starting to show some deviation from the BGO differential spectrum. The ratio of the integral electron fluxes J(>1.01,BGO)/J(>1.01,S2B) is 1.83. In Figure 26 the electron intensity is about a factor of 3 greater, with large deadtime correction factors, and the SSDF (S1F-S2F) differential spectrum point is clearly meaningless. The SSDB (S1B-S2B) differential spectrum point is low compared with the BGO differential spectrum, but this may be partly the result of a flattening of the low energy part (<1 MeV) of the electron spectrum. The ratio of the integral electron fluxes J(>1.01,BGO)/ J(>1.01,S2B) is 2.53.

Figure 27 show a second spectrum for orbit 600, L = 4.48, but for pitch angles of 0° and 180°. Here, the electron flux is weaker by about a factor of 10, so the deadtime corrections are not as large. The SSDF differential spectrum point is now in better agreement with the BGO differential spectrum, and the integral flux ratio J(>1.01,BGO)/J(>1.01,S2B) is 2.81. The integral flux ratio is thus not strongly dependent on the electron flux intensity, and indicates that the BGO corrections are being made correctly. The deviation of J(>1.01,BGO) from J(>1.01,S2B) is most likely due to

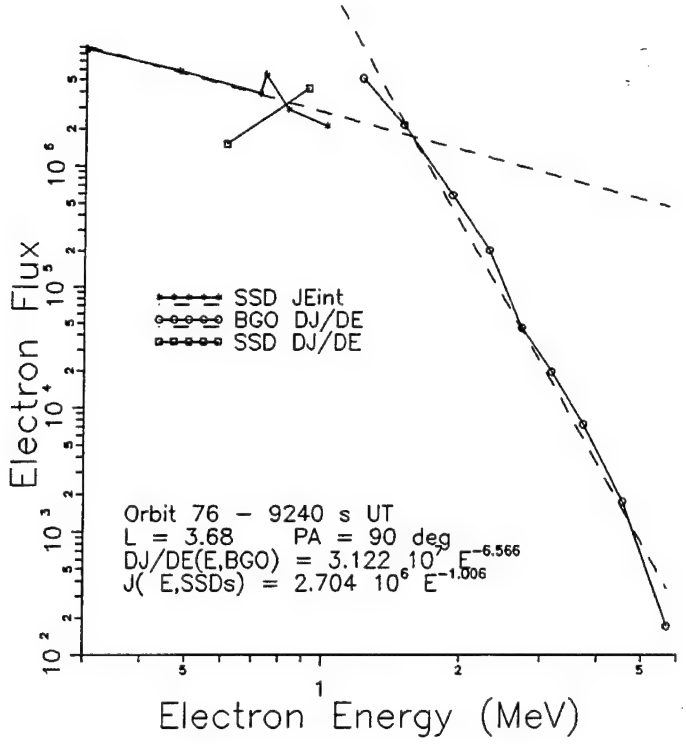

Figure 20. HEEF Electron Spectrum for Orbit 76, L = 3.68.

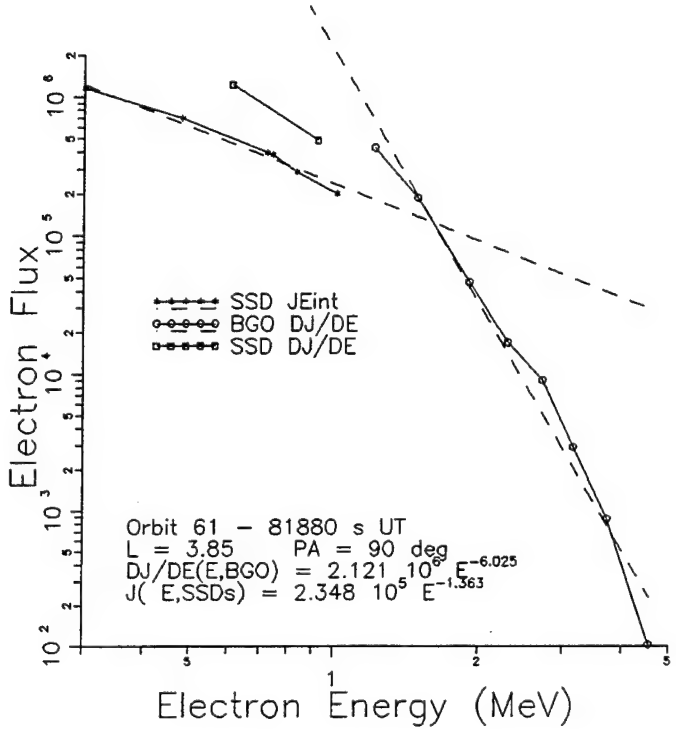

Figure 21. HEEF Electron Spectrum for Orbit 61, L = 4.1.

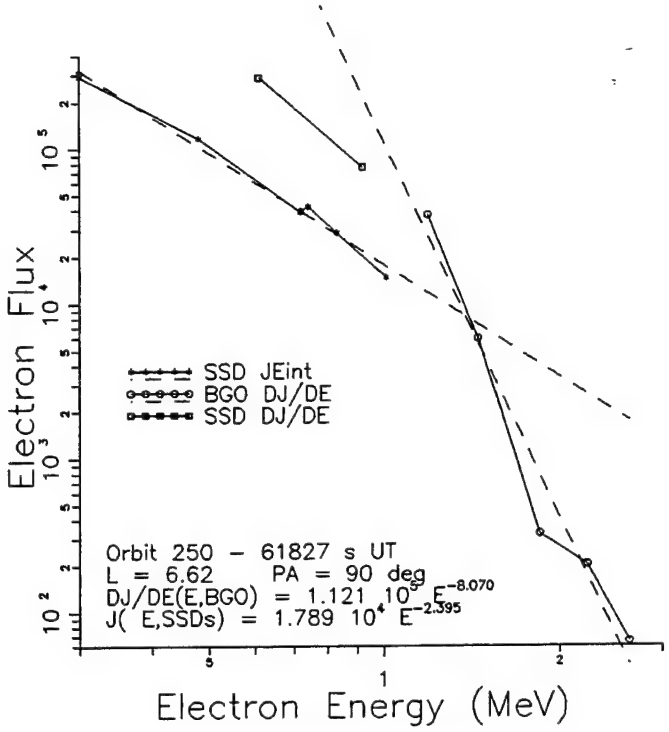

Figure 22. HEEF Electron Spectrum for Orbit 250, L = 6.62.

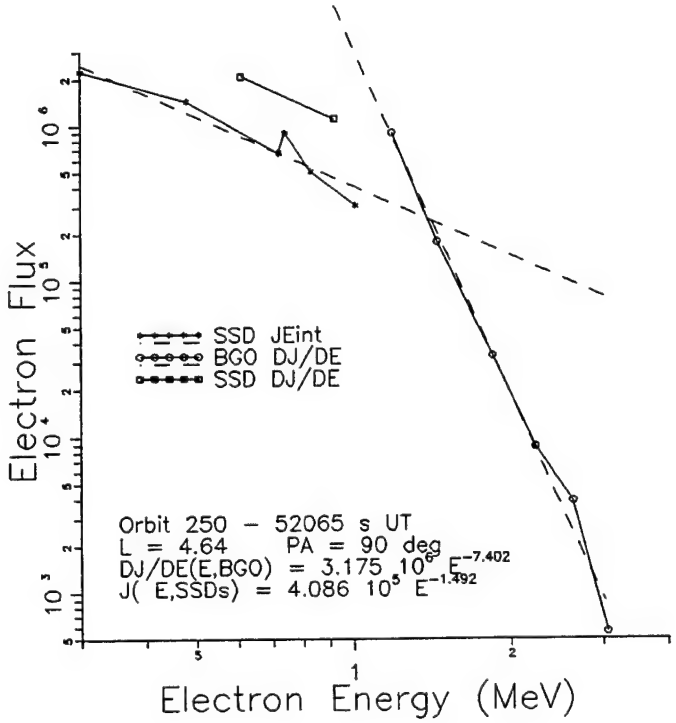

Figure 23. HEEF Electron Spectrum for Orbit 250, L = 4.64.

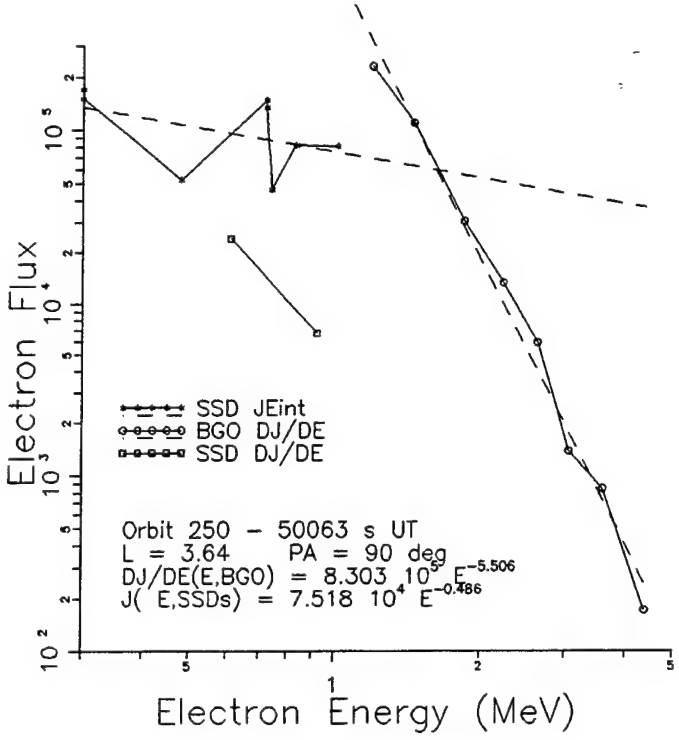

Figure 24. HEEF Electron Spectrum for Orbit 250, L = 3.64.

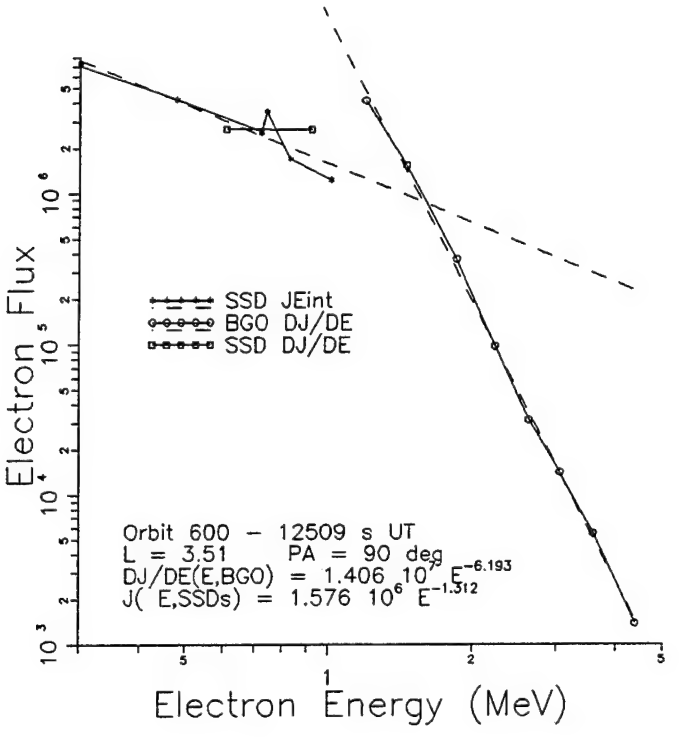

Figure 25. HEEF Electron Spectrum for Orbit 600, L = 3.51.

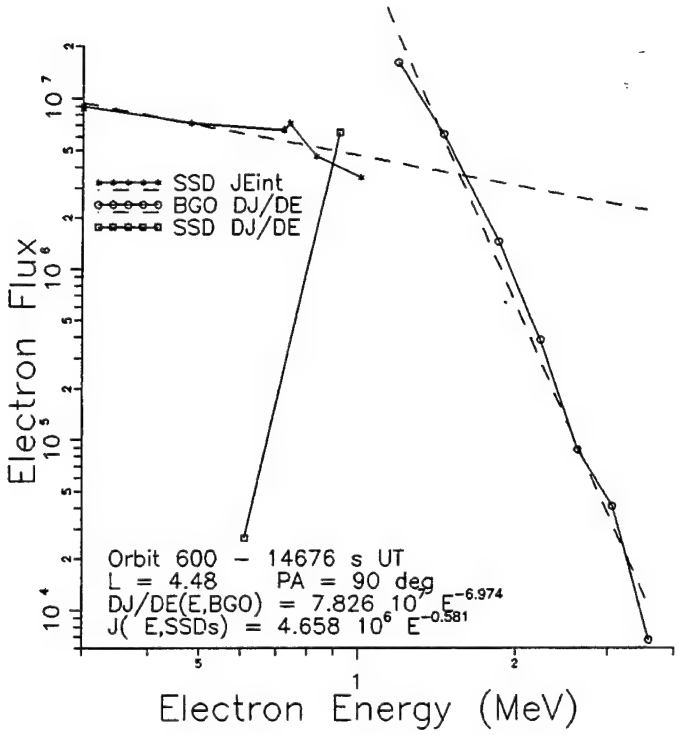

Figure 26. HEEF Electron Spectrum for Orbit 600, L = 4.48.

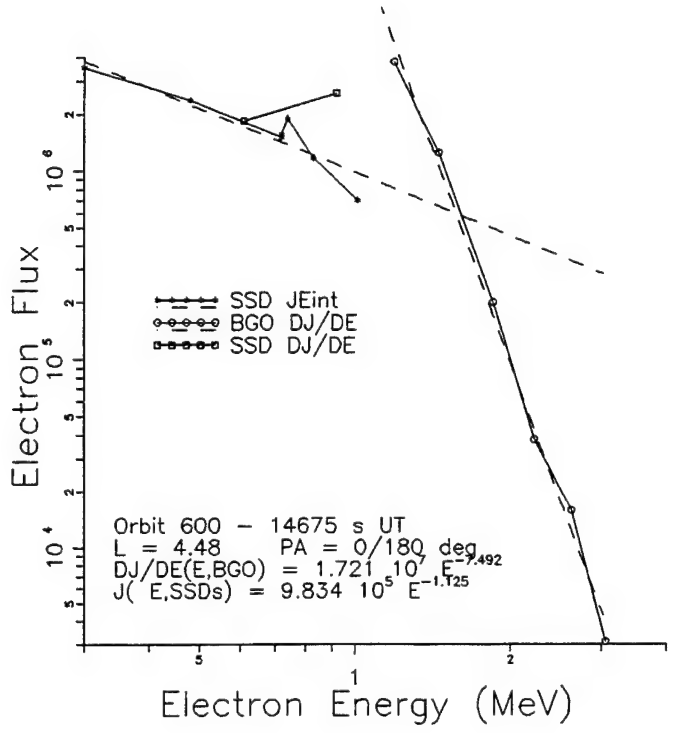

Figure 27. HEEF Electron Spectrum for Orbit 600, L = 4.48, PA = 0°/180°.

electron spectrum shape effects, with the spectrum below about 1 MeV being much flatter than that above 1 MeV.

Electron spectra for orbit 600, L = 5.49, and orbit 602, L = 3.11, are shown in Figures 28 and 29. Both spectra are similar in shape and intensity, and the BGO spectra show moderate agreement with the SSDB differential spectrum point at 0.92 MeV, but significant disagreement with the SSDF differential spectrum point at 0.61 MeV. The total SSDF count rates are about 1 MHz for both spectra, so the SSDF deadtime corrections are moderately large. The integral electron flux ratios J(>1.01,BGO)/J(>1.01,S2B) are 2.56 for orbit 600 (Figure 28) and 2.08 for orbit 602 (Figure 29), so the ratio does not vary much for this time period.

Much of the HEEF data were obtained with the sensor temperature near -10°C (nearly all orbits above 130), where the effective detection efficiency is only a few %. Changing the sensor temperature to -15°C decreases the BGO geometric factors by a factor of 2 for channel LL, and about a factor of 5 for L8 and L9. The BGO geometric factors near -10°C are thus strongly temperature dependent, and some of the deviations of J(>1.01,BGO) from J(>1.01,S2B) may be the result of slight differences between the actual HEEF sensor temperature and the temperature used for the flux calculations. The calculations shown in Figures 16 to 29 use average HEEF sensor temperatures for the orbits in question, and thus there is a possibility that some of the actual sensor temperatures were slightly different.

The HEEF electron data appear to be quite accurate when all the deadtime corrections are made, and when the correct sensor temperature is used to obtain the BGO channel geometric factors. The agreement between the BGO and SSD electron fluxes is generally quite good, and can be used as a check on correct data reduction. The SSD data are not useful when there are significant proton fluxes present, since the proton response adds to the electron response. Correction of the SSD response for small proton flux contributions is possible, but once the proton flux response is greater than the electron flux response the SSD data are not too useful for calculating the lower energy electron spectrum.

4.2 Measured Dosimeter Doses and Particle Fluxes

The dosimeter data from CRRES is analyzed as described in Section 2, and is much the same procedure used for the DMSP/F7 dosimeter. The bulk of the data reduction has been done at PL, with the data being used to generate dose rate information for the parts of the magnetosphere measured by CRRES. The dosimeter provides accurate dose measurements for the detector and shielding geometries used, since the sensitive silicon volume has been accurately measured and the output pulse energy scale has been accurately calibrated. Because the dosimeter has a nearly 2π sr response in its primary energy ranges, the particle flux measurements are integrations over the entire pitch angle distribution and detailed particle flux measurements are not

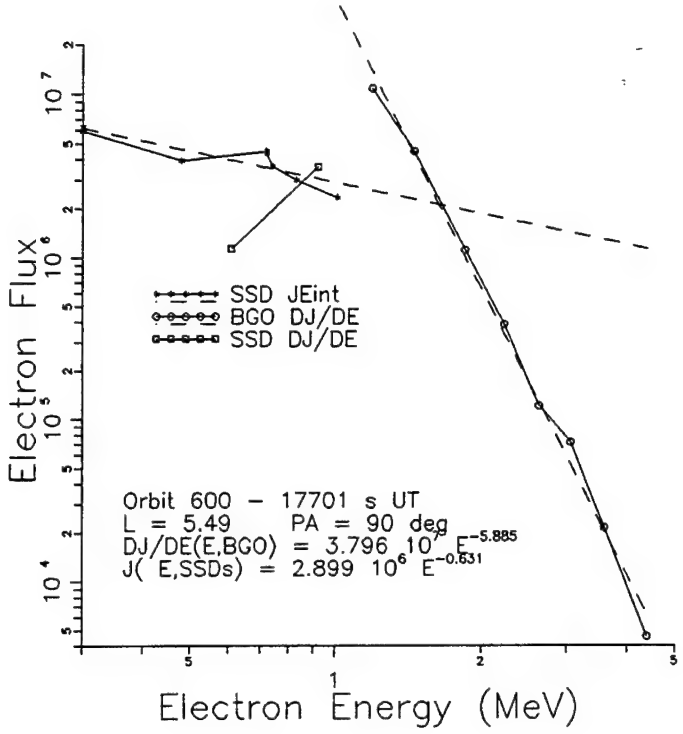

Figure 28. HEEF Electron Spectrum for Orbit 600, L = 5.49.

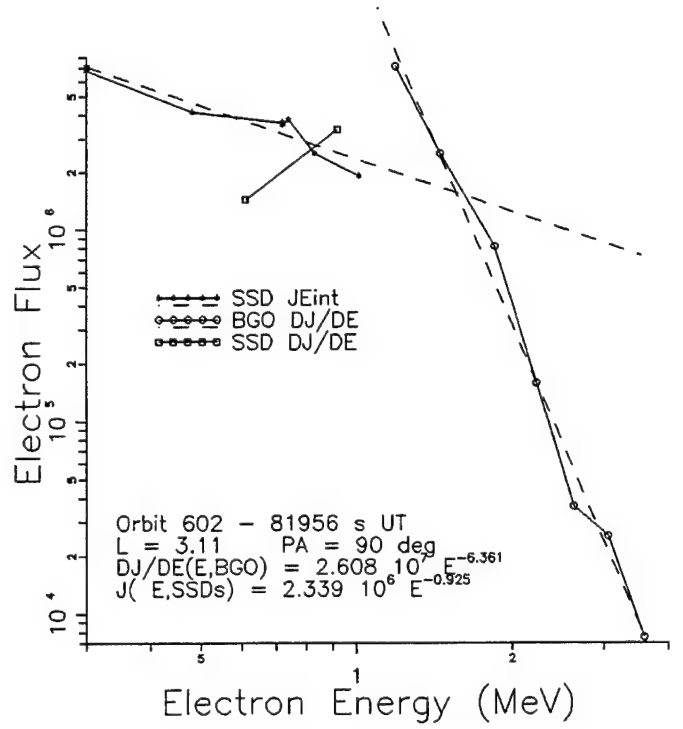

Figure 29. HEEF Electron Spectrum for Orbit 602, L = 3.11.

possible. The flux data can be used to provide estimates of the average omnidirectional particle fluxes.

The dose rate data and the particle flux data can be used to calculate the average energy deposited by one particle in a particular dose channel. In the LOLET (Ei) channels this allows some discrimination between response to protons (average energy loss is usually above 300 keV), electrons (average energy loss is about 200 keV) and electron bremsstrahlung (average energy loss is less than about 100 keV). The HILET (Pi) channels respond primarily to protons, although there is a very weak response to high energy electrons due to multiple scattering in the SSDs. The HILET channels have a typical average energy loss of a few MeV. For very low ambient particle fluxes, the dosimeter data must have the calibration source background subtracted (Reference 1). Note that since the P4 flux channel has a prescale of 8 before the telemetry output, all P4 flux counts from telemetry must be multiplied by 8 to obtain the actual SSD P4 flux count. All dosimeter P4 flux data shown here have had this factor of 8 applied to the telemetry P4 flux counts.

The dosimeter calibration mode is used to verify the SSD total depletion and the overall electronics gain and operation. Calibration mode data are useable only when the ambient particle fluxes are low, especially the proton fluxes which produce HILET doses. Calibration mode data are thus useable only near perigee, and at very high L values during quiet magnetospheric times. Calibration mode data for several orbits covering nearly the entire lifespan of CRRES are given in Table 37. Comparing the in-orbit data with the pre-launch values of flux count rate, dose count rate, and average deposited energy shows good agreement from orbit 6 up to orbit 1021, and verifies proper dosimeter operation for the entire CRRES operational lifetime. The E1(Cal mode) data show a slight contamination from ambient particles, since the in-orbit flux count rates are slightly higher than the pre-launch values. However, the P1(Cal mode) data show very good agreement between in-orbit and pre-launch values, and this is the primary indication of total SSD depletion and proper electronics operation.

Dosimeter normal mode data at high L values during quiet magnetospheric conditions are given in Table 38. The pre-launch values provide the dosimeter background flux/dose count rates from the calibration sources, and must be used to correct the in-orbit data when the ambient particle fluxes are low. The E1 channel has the lowest energy threshold, and thus almost always has some count rate from ambient particles. Thus, the in-orbit E1 count rate is almost always higher than the pre-launch value. Only in orbits 6 and 250 does the E1 in-orbit flux count rate come very close to the pre-launch value. The normal mode data in Table 38 help verify proper in-orbit dosimeter operation, since all in-orbit count rate data are equal to or greater than the pre-launch values.

Dosimeter in-orbit data for CRRES are illustrated by the summaries in Tables 39 to 42, which are for the outbound half of orbit 76. The data listed have no deadtime corrections, but this

Table 37: CRRES Dosimeter Calibration Mode Data

Chan	Pre-launch values (vac)			Orbit 6 values/L = 7.0			Orbit 600 values/L = 6.6		
	Flux/cps	Dose/cps	ΔE/MeV	Flux/cps	Dose/cps	ΔE/MeV	Flux/cps	Dose/cps	ΔE/MeV
E1	0.82	9.1	2.22	1.09	11.9	2.19	1.91	17.1	1.79
E2	0.28	3.0	2.14	0.267	2.69	2.02	1.47	8.86	1.20
E3	0.36	4.5	2.50	0.398	4.59	2.31	0.356	4.01	2.25
E4	0.60	6.2	2.07	0.863	8.36	1.94	0.980	9.63	1.97
P1	1.57	2.4	3.06	1.57	2.39	3.04	1.75	2.65	3.03
P2	0.25	0.37	2.96	0.207	0.336	3.25	0.268	0.445	3.32
P3	0.45	0.68	3.02	0.540	0.845	3.13	0.547	0.859	3.14
P4	0.928	1.46	3.15	0.996	1.64	3.28	0.929	1.58	3.41

Chan	Orbit 956 values/L = 1.1			Orbit 972 values/L = 1.1			Orbit 1021 values/L = 1.1		
	Flux/cps	Dose/cps	ΔE/MeV	Flux/cps	Dose/cps	ΔE/MeV	Flux/cps	Dose/cps	ΔE/MeV
E1	1.25	13.8	2.20	1.16	12.5	2.17	1.28	13.7	2.14
E2	0.304	3.06	2.02	0.248	2.36	1.91	0.234	2.58	2.20
E3	0.330	3.76	2.28	0.301	3.47	2.30	0.348	3.57	2.05
E4	0.792	8.46	2.14	0.756	8.12	2.15	0.776	8.68	2.24
P1	1.66	2.56	3.07	1.82	2.64	2.90	1.56	2.31	2.97
P2	0.264	0.410	3.11	0.197	0.302	3.06	0.258	0.382	2.97
P3	0.469	0.732	3.13	0.485	0.725	2.99	0.565	0.846	2.99
P4	0.818	1.43	3.49	0.803	1.48	3.69	0.856	1.59	3.71

Table 38: CRRES Dosimeter Normal Mode Data

Chan	Pre-launch values (air)			Orbit 6 values/L = 6-7			Orbit 780 values/L = 6.6		
	Flux/cps	Dose/cps	ΔE/MeV	Flux/cps	Dose/cps	ΔE/MeV	Flux/cps	Dose/cps	ΔE/MeV
E1	0.392	2.63-4	0.378	0.480	3.20-4	0.375	1.38	7.08-4	0.289
E2	0.0681	4.47-5	0.392	0.356	1.23-4	0.206	1.38	7.33-4	0.316
E3	0.0569	5.07-5	0.491	0.313	1.16-4	0.204	0.872	5.25-4	0.332
E4	0.1363	4.05-5	0.351	1.53	5.27-4	0.406	1.74	8.67-4	0.587
P1	2.32	4.34-2	2.89	2.67	5.10-2	2.95	3.04	5.67-2	2.89
P2	0.509	2.12-3	2.58	0.530	2.46-3	2.89	0.791	3.42-3	2.69
P3	0.734	6.65-3	2.79	0.874	8.44-3	2.97	1.04	1.01-2	2.98
P4	1.50	8.94-4	2.90	1.73	1.06-3	2.99	2.91	1.61-3	2.71

Chan	Orbit 550 values/L= 6.6			Orbit 250 values/L = 7-8			Orbit 972 values/L = 6.6		
	Flux/cps	Dose/cps	ΔE/MeV	Flux/cps	Dose/cps	ΔE/MeV	Flux/cps	Dose/cps	ΔE/MeV
E1	1.062	5.52-4	0.293	0.465	3.32-4	0.402	1.08	5.40-4	0.282
E2	0.386	1.67-4	0.259	0.287	1.17-4	0.243	0.678	1.49-4	0.131
E3	0.330	1.67-4	0.279	0.229	1.12-4	0.270	0.639	1.59-4	0.137
E4	1.88	7.47-4	0.470	1.77	6.32-4	0.422	1.23	6.17-4	0.593
P1	2.95	5.51-2	2.89	2.92	5.49-2	2.91	2.84	5.30-2	2.89
P2	0.519	2.34-3	2.80	0.523	2.32-3	2.76	0.513	2.31-3	2.80
P3	0.867	8.52-3	3.02	0.857	8.52-3	3.06	0.862	8.56-3	3.06
P4	1.78	1.17-3	3.21	1.78	1.11-3	3.04	1.76	1.08-3	3.00

should not affect the general pattern of the dosimeter data. The last set of entries give the calibration source count rates and average energy deposits (ΔE), taken from Table 38.

The data for channel 1 in Table 39 show the expected response pattern for the radiation belts. The inner belt point at L = 1.55 shows a high LOLET energy deposit (308 keV) typical of proton response in the inner belt. The average energy deposit drops to 152.4 keV at L = 2.38, which indicates a significant response to bremsstrahlung from an intense electron flux with energies below about 1 MeV. For all of the higher L values the average energy deposit is about 200 keV, which corresponds to a primary response to high energy electrons. The HILET channel response shows a typical proton response at L = 1.55, a small electron response at L = 3.86 where the average energy deposit drops to 1.87 MeV, and a dominant calibration source response for most of the high L values.

The channel 2 response in Table 40 shows a pattern similar to that for channel 1, although the inner belt proton response produces a slightly higher average LOLET energy deposit of 372 keV because of the larger detector area. At the highest L values the LOLET response is partly bremsstrahlung, as shown by the lower average energy deposit values. The HILET response is very similar to the channel 1 HILET response: protons at L = 1.55, some electron response at L = 3.86, and calibration source response at the highest L values.

The channel 3 response in Table 41 shows the expected LOLET proton response at L = 1.55, and a dominant bremsstrahlung response at all higher L values. There is a slight direct electron response at L values of 3.86 and 4.64, as shown by the elevated average energy deposits of 110.6 and 105.7 keV. The HILET channel response is to protons at the lowest L values of 1.55 and 2.38, and almost entirely to the calibration source for all higher L values.

The channel 4 response in Table 42 is very similar to the channel 3 response, except that the LOLET average energy deposits are higher because of the much larger detector area. The response outside of the inner belt is basically all bremsstrahlung. The HILET response outside of the inner belt is somewhat higher than from the calibration source alone, and is a combination of cosmic ray proton background and electron bremsstrahlung.

The dosimeter data indicate that the instrument has operated properly for the entire operational life of CRRES. The calibration source data, both Calibration Mode and Normal Mode (low ambient particle background), show that all detectors operated properly, and that all electronic gains and operations were correct. Data from the radiation belts show the expected responses from the proton and electron fluxes.

Table 39: Dosimeter Data Summary for Channel 1 for Orbit 76 Outbound					
Average L Value	L Value Range	LOLET (E1) Averages		HILET (P1) Averages	
		Flux (cps)	ΔE (keV)	Flux (cps)	ΔE (MeV)
1.55	1.24/1.85	160.2	308.0	96.9	2.99
2.38	1.85/2.92	39.0	152.4	5.67	3.05
3.20	2.93/3.46	3947.	209.6	3.10	2.61
3.86	3.46/4.26	15420.	205.3	5.03	1.87
4.64	4.26/5.01	6412.	208.3	3.47	2.46
5.43	5.02/5.83	1365.	211.7	2.92	2.81
6.10	5.83/6.36	275.7	213.8	2.79	2.92
6.47	6.37/6.56	93.7	213.5	2.76	2.92
Cal Src	(All)	0.392	378.	2.32	2.89

Table 40: Dosimeter Data Summary for Channel 2 for Orbit 76 Outbound					
Average L Value	L Value Range	LOLET (E2) Averages		HILET (P2) Averages	
		Flux (cps)	ΔE (keV)	Flux (cps)	ΔE (MeV)
1.55	1.24/1.85	341.8	372.2	182.8	2.52
2.38	1.85/2.92	121.5	95.7	4.56	2.66
3.20	2.93/3.46	525.3	185.0	1.24	2.01
3.86	3.46/4.26	1683.	224.3	3.52	1.35
4.64	4.26/5.01	698.	221.4	1.71	1.46
5.43	5.02/5.83	140.3	191.9	0.74	2.53
6.10	5.83/6.36	32.8	145.6	0.57	2.53
6.47	6.37/6.56	14.23	116.9	0.53	2.86
Cal Src	(All)	0.0681	392.	0.509	2.58

Table 41: Dosimeter Data Summary for Channel 3 for Orbit 76 Outbound					
Average L Value	L Value Range	LOLET (E3) Averages		HILET (P3) Averages	
		Flux (cps)	ΔE (keV)	Flux (cps)	ΔE (MeV)
1.55	1.24/1.85	291.1	377.7	109.8	2.20
2.38	1.85/2.92	85.6	89.4	2.70	2.53
3.20	2.93/3.46	182.6	93.9	0.90	3.09
3.86	3.46/4.26	317.0	110.6	0.88	3.09
4.64	4.26/5.01	138.3	105.7	0.86	2.87
5.43	5.02/5.83	45.9	96.2	0.87	3.08
6.10	5.83/6.36	17.45	94.7	0.85	3.00
6.47	6.37/6.56	8.95	89.1	0.86	3.03
Cal Src	(All)	0.0569	491.	0.734	2.79

Table 42: Dosimeter Data Summary for Channel 4 for Orbit 76 Outbound					
Average L Value	L Value Range	LOLET (E4) Averages		HILET (P4) Averages	
		Flux (cps)	ΔE (keV)	Flux (cps)	ΔE (MeV)
1.55	1.24/1.85	2216.	590.2	1161.	2.37
2.38	1.85/2.92	155.8	244.3	15.20	2.51
3.20	2.93/3.46	698.	239.4	1.87	2.62
3.86	3.46/4.26	1680.	258.8	2.17	2.66
4.64	4.26/5.01	693.	253.6	1.95	2.52
5.43	5.02/5.83	193.0	240.9	1.78	3.67
6.10	5.83/6.36	61.3	237.5	1.79	2.73
6.47	6.37/6.56	26.86	234.9	1.74	3.13
Cal Src	(All)	0.1363	351.	0.188	2.90

4.3 Comparison of HEEF and Dosimeter Electron Flux Data

4.3.1 Method to Calculate Dosimeter Electron Flux Responses from HEEF Electron Flux Data

The electron fluxes calculated from HEEF on CRRES can be used to calculate the Dosimeter LOLET (electron) flux count rates. In principal the HEEF fluxes should be integrated over pitch angle to provide an omnidirectional flux for electrons, but in practice the 90° pitch angle data can be used since they are usually within 25% or so of the true omnidirectional flux. The Dosimeter has a 4.096 second integration time and a FOV near 2π sr, so it shows only a small variation with the FOV center pitch angle, but it is still desirable to average the Dosimeter flux count rates over a full satellite spin.

The direct electron flux count rate of a particular dosimeter LOLET channel (E1, E2, E3 and E4) is calculated from

$$R_{fe} = \Sigma\ j_e(E_i) * DE_i * G_{fe}(E_i) \qquad (4.1)$$

where the sum is over the electron energies E_i, and

E_i, DE_i = central energy and bin width of the HEEF electron energy channels, in MeV

$j_e(E_i)$ = HEEF differential electron flux, $DJ/DE(E_i)$, in $el/(cm^2\ s\ sr\ MeV)$

$G_{fe}(E_i)$ = Dosimeter channel geometric factor for electrons of energy E_i, in cm^2 sr

The values of $G_{fe}(E_i)$ for the four Dosimeter channels are calculated using Eq. (2.1) for the CRRES dosimeter SSD areas and threshold energies of Table 3. Note that the sum in Eq. (4.1) is approximate for steeply falling electron spectra (E_e^{-6} or so), where an integral over the response would be more accurate.

The dosimeter LOLET channels also respond to electron bremsstrahlung, and this is frequently the dominant response for the D3 and D4 LOLET channels E3 and E4. The dosimeter response to bremsstrahlung can be calculated from the HEEF SSD integral electron channels, since most of the bremsstrahlung come from electrons below about 1 MeV. A five-point integral electron spectrum can be obtained from HEEF by using the effective threshold channels listed in Table 19. The five points are obtained from

$J_e(E_e > 0.30$ MeV)	- W1F and W2F average
$J_e(E_e > 0.48$ MeV)	- S1F
$J_e(E_e > 0.72$ MeV)	- W1B and W2B average
$J_e(E_e > 0.83$ MeV)	- S1B
$J_e(E_e > 1.01$ MeV)	- S2B

where the S2F point at 0.74 MeV is not used since it is very close to the W1B + W2B point. The bremsstrahlung response is calculated

from

$$R_{be} = \Sigma \ (J_e(E_{i+1}) - J_e(E_i)) * 4\pi * G_{omni}((E_{i+1} + E_i)/2) \qquad (4.2)$$

where the sum is over the integral electron energies E_i, $J_e(E_i)$ are the HEEF integral electron fluxes, and $G_{omni}(E_e)$ are the interpolated dosimeter bremsstrahlung cross sections from Table 6 (fourth column, labeled "CRRES"). Note that Eq. (4.2) calculates the bremsstrahlung response only for electrons >0.30 MeV, and uses the HEEF SSD electron spectra which may have proton flux contamination. At very high flux levels the SSDF data (W1F, W2F and S1F) may have large uncertainties because of large deadtime corrections (see Sections 3.3 and 3.4).

4.3.2 Comparison of Measured Dosimeter Electron Responses with Calculations from HEEF Data

The measured dosimeter LOLET (electron channel) count rates are compared with the calculated count rates using the measured HEEF electron spectra in Figures 16 to 26 and Figure 29. (Figure 27 is a different pitch angle measurement for the same location as Figure 26, and there are no dosimeter data for Figure 28 since the dosimeter was in Cal Mode at that time.) The results are summarized in Tables 43 to 46 for the four channels E1, E2, E3 and E4.

The E1 results in Table 43 give two sets of dosimeter response calculations, one for the E1 SSD areas and threshold energies of Table 3, and a second for a modified E1 electron response, based on the calibrated data of the D2A electron channel of the PASP Plus dosimeter (Reference 9). The PASP Plus dosimeter D2A channel has the same detector size and shield thickness as the CRRES dosimeter D1 dome. The modified E1 geometric factor for electrons is given by

$$\begin{aligned} G_{fe1}(E) &= 0 && E/T_1 < 1 \\ &= 7.38 \times A_{1o} \times (1 - T_1/E)^2 && 1 \le E/T_1 \le 5.449 \\ &= 4.92 \times A_{1o} && E/T_1 \ge 5.449 \end{aligned} \qquad (4.3)$$

with $A_{1o} = 0.0170$ cm^2 and $T_1 = 1.20$ MeV. The form (4.3) fits the data of Reference 9 to about ±25%. The reason for the difference between the calibration results of Reference 9 and those in References 2 and 7 is not clear, but the Reference 2 data were taken with a comparatively broad energy spread electron beam, and this combined with a significant bremsstrahlung background from higher energy electrons may account for the difference.

The results in Table 43 include the bremsstrahlung response, which is generally less than about 1% for all the spectra listed. The responses calculated with $G_{fe1}(E)$ from Eq. (2.1) average to a calculated/measured ratio of 4.88, while the responses using $G_{fe1}(E)$ from Eq. (4.3) average to 0.456. These results show that the modified geometric factor (4.3) gives a better agreement between

the HEEF-calculated responses and the measured dosimeter responses. Thus the CRRES HEEF data indicate that the Reference 9 calibrations are more accurate.

Table 44 gives the dosimeter E2 channel comparisons with the HEEF spectrum calculations. The direct electron response is given as well as the response which includes the electron bremsstrahlung. For the dosimeter E2 channel the bremsstrahlung response is sometimes a significant part of the total flux count rate. The average calculated/measured response is 1.197 for the electron response only, and 1.290 for the total (electron + bremsstrahlung) response. The E2 channel thus shows good agreement with the HEEF spectrum calculations, although the data in Table 44 show variations of at least a factor of two from the average.

Table 45 gives the dosimeter E3 channel comparisons with the HEEF calculations, which is essentially all bremsstrahlung response. The last column gives a required bremsstrahlung response factor, which would bring the calculated response into agreement with the measured response. The average calculated/measured response ratio is 0.205, and the average required bremsstrahlung factor is 5.49. From Table 6 it can be seen that the Reference 8 bremsstrahlung response calculations for E3 are about 50% larger than the CRRES values based on Reference 7, which latter are used in the present calculations, and use of the Reference 8 calculations would give slightly better agreement. Uncertainties in the calculated dosimeter electron channel bremsstrahlung responses may thus account for much of the observed disagreement with the calculations based on the measured HEEF electron spectra. It should be noted, however, that the present bremsstrahlung responses are calculated only for electrons above 0.3 MeV using the HEEF SSD data, and thus an intense flux of lower energy electrons could account for some of the observed higher E3 count rates.

Table 46 gives the dosimeter E4 channel comparisons with the HEEF calculations, which is all bremsstrahlung response since HEEF has no data points above 10 MeV. As for E3 in Table 45, the last column gives a required bremsstrahlung response factor. The average calculated/measured response ratio is 0.770, and the average required bremsstrahlung factor is 1.660, so the HEEF and dosimeter data are in reasonable agreement. From Table 6, it can be seen that the Reference 8 bremsstrahlung response calculations for E4 compared with the CRRES values based on Reference 7 are about a factor of 2 smaller at 0.3 MeV and about the same at 1 MeV. Also, the present bremsstrahlung responses are calculated only for electrons above 0.3 MeV using the HEEF SSD data.

The comparison of the measured dosimeter LOLET (electron - E1, E2, E3 and E4) channel flux count rates with those calculated from the measured HEEF electron spectra are in moderate agreement. The comparisons indicate that the two instruments agree to within about a factor of two on the electron spectrum. This is within the uncertainties of the dosimeter electron calibration data and the calculated bremsstrahlung responses, the uncertainties in the HEEF geometric factors because of the temperature variations, the use of

Table 43: Comparison of Dosimeter E1 Channel Measured Responses with HEEF Electron Spectrum Calculated Responses						
HEEF Spectrum Figure	CRRES Orbit No.	L Value	J(>1.01,S2B) (el/(cm^2 s sr))	J(>1.01,BGO) / J(>1.01,SSD)	Calculated Response / Measured Response	
					$G_{fe1}(E)$ (2.1)	$G_{fe1}(E)$ (4.3)
16	75	5.36	1.683×10^5	1.081	3.60	0.392
17	76	6.75	1.823×10^4	0.932	5.09	0.489
18	20	3.47	8.988×10^5	1.348	4.76	0.618
19	12	3.17	6.574×10^5	1.075	7.32	0.465
20	76	3.68	2.112×10^6	1.480	4.18	0.491
21	61	3.85	2.000×10^5	1.328	4.31	0.543
22	250	6.58	2.448×10^4	1.322	4.66	0.236
23	250	4.64	3.061×10^5	1.609	5.16	0.294
24	250	3.64	8.074×10^4	1.689	3.01	0.401
25	600	3.51	1.227×10^6	1.832	4.92	0.467
26	600	4.48	3.456×10^6	2.527	6.47	0.582
29	602	3.11	1.908×10^6	2.078	5.04	0.488

Table 44: Comparison of Dosimeter E2 Channel Measured Responses with HEEF Electron Spectrum Calculated Responses

HEEF Spectrum Figure	CRRES Orbit No.	L Value	J(>1.01,S2B) (el/(cm^2 s sr))	J(>1.01,BGO) / J(>1.01,SSD)	Calculated Response / Measured Response	
					Only Direct Electron	Includes Bremsstrahlung
16	75	5.36	1.683×10^5	1.081	1.050	1.143
17	76	6.75	1.823×10^4	0.932	0.951	1.176
18	20	3.47	8.988×10^5	1.348	2.498	2.572
19	12	3.17	6.574×10^5	1.075	0.466	0.711
20	76	3.68	2.112×10^6	1.480	1.873	1.916
21	61	3.85	2.000×10^5	1.328	2.493	2.543
22	250	6.58	2.448×10^4	1.322	0.336	0.515
23	250	4.64	3.061×10^5	1.609	0.467	0.590
24	250	3.64	8.074×10^4	1.689	1.325	1.333
25	600	3.51	1.227×10^6	1.832	0.838	0.862
26	600	4.48	3.456×10^6	2.527	1.219	1.251
29	602	3.11	1.908×10^6	2.078	0.846	0.867

Table 45: Comparison of Dosimeter E3 Channel Measured Responses with HEEF Electron Spectrum Calculated Responses

HEEF Spectrum Figure	CRRES Orbit No.	L Value	J(>1.01,S2B) (el/(cm^2 s sr))	J(>1.01,BGO) / J(>1.01,SSD)	Calculated Response / Measured Response	
					Electron + Bremsstrahlung	Required Brems Factor
16	75	5.36	1.683×10^5	1.081	0.248	4.03
17	76	6.75	1.823×10^4	0.932	0.278	3.60
18	20	3.47	8.988×10^5	1.348	0.181	5.54
19	12	3.17	6.574×10^5	1.075	0.292	3.42
20	76	3.68	2.112×10^6	1.480	0.231	5.17
21	61	3.85	2.000×10^5	1.328	0.198	5.06
22	250	6.58	2.448×10^4	1.322	0.247	4.05
23	250	4.64	3.061×10^5	1.609	0.224	4.47
24	250	3.64	8.074×10^4	1.689	0.089	11.23
25	600	3.51	1.227×10^6	1.832	0.175	5.70
26	600	4.48	3.456×10^6	2.527	0.145	6.88
29	602	3.11	1.908×10^6	2.078	0.149	6.70

Table 46: Comparison of Dosimeter E4 Channel Measured Responses with HEEF Electron Spectrum Calculated Responses

HEEF Spectrum Figure	CRRES Orbit No.	L Value	J(>1.01,S2B) (el/(cm^2 s sr))	J(>1.01,BGO) / J(>1.01,SSD)	Calculated Response / Measured Response	
					Electron + Bremsstrahlung	Required Brems Factor
16	75	5.36	1.683×10^5	1.081	0.836	1.196
17	76	6.75	1.823×10^4	0.932	1.513	0.661
18	20	3.47	8.988×10^5	1.348	0.514	1.945
19	12	3.17	6.574×10^5	1.075	1.183	0.846
20	76	3.68	2.112×10^6	1.480	0.504	1.984
21	61	3.85	2.000×10^5	1.328	0.582	1.718
22	250	6.58	2.448×10^4	1.322	0.908	1.102
23	250	4.64	3.061×10^5	1.609	0.751	1.331
24	250	3.64	8.074×10^4	1.689	0.198	5.053
25	600	3.51	1.227×10^6	1.832	0.919	1.088
26	600	4.48	3.456×10^6	2.527	0.655	1.528
29	602	3.11	1.908×10^6	2.078	0.680	1.471

only the 90° pitch angle spectra, and the use of a sum in Eq. (4.1) for steeply falling spectra.

5. Modification of Backup HEEF

The HEEF SN/1 launched on CRRES provided much useful electron flux data, but because of the low operating temperature for most of the spacecraft life the actual geometric factors for the BGO triple coincidence data were only a few % of the room temperature values. It would be a significant improvement for HEEF to have a larger geometric factor at low temperature. Also, data from the inner belt indicate that penetrating protons are not a problem for the BGO scintillator, with the background count rates not being a significant deadtime source, while data in regions of intense electron flux show that electron bremsstrahlung also is not a problem for the BGO scintillator, with background count rates not being a significant deadtime source. Thus, it should be possible to reduce the sensor mass by removal of some of the tungsten shielding.

The backup HEEF SN/2 has been modified to deal with the BGO temperature effects so that it will operate with near constant triple coincidence efficiency over the range of 30°C to -20°C. The mass of the HEEF sensor can also be reduced by nearly half by removing all of the tungsten shielding and replacing it with aluminum. The FOV collimation for the front solid state detector (SSDF) can also be improved significantly to reduce the very high count rates, and resulting severe deadtime effects, measured on CRRES. These actual, and possible, modifications are discussed below.

5.1 Modification of BGO Coincidence Pulse Width

The electron spectral detection of HEEF comes from a triple coincidence between SSDF, SSDB and BGO. To reduce accidental coincidences to a minimum it is necessary to make the coincidence resolving time as narrow as possible. For the original HEEF design the three triple coincidence timing pulses were about 85 ns wide, with circuits that require about a 20 ns overlap to trigger the triple coincidence output pulse. This produces a nominal coincidence time resolution of about 130 ns for any pulse pair. Timing data taken with HEEF SN/1 are shown in Figure 30, and give measured FWHM coincidence timing resolutions of 112 ns for SSDF/SSDB, 103 ns for SSDF/BGO, and 101 ns for SSDB/BGO.

At room temperature (about 20°C) the timing was set with electrons from a Ru-Rh-106 beta source so that all three pulses overlap optimally, for a maximum triple coincidence detection efficiency. At low temperatures the BGO light pulse decay time increases, and this results in a slight shift of the zero-cross generated BGO timing pulse. The result, discussed in Reference 5, is that at low temperature the triple coincidence efficiency becomes very low (a few % at -10°C). The measured data at low temperature show that the BGO timing pulse has shifted about 100 ns

later in time at -20°C. To counter this BGO pulse shift, the BGO timing pulse was widened to about 160 ns, and the SSDF and SSDB timing pulses were delayed by about 80 ns. This arrangement allows for the temperature/time shift of the BGO timing pulse by increasing the width of only the BGO timing pulse, thus minimizing the increase in accidental coincidence count rates.

Timing data taken with the modified HEEF SN/2 are shown in Figure 31, and give measured FWHM coincidence timing resolutions of 119 ns for SSDF/SSDB, 179 ns for SSDF/BGO, and 175 ns for SSDB/BGO. Tests with Ru-Rh-106 beta source electrons at +30°C and at -20°C show that the triple coincidence detection efficiency is nearly the same at both temperatures. HEEF SN/2 should thus operate reliably over at least this temperature range. This change should allow for in-orbit count rates that are at least a factor of 20 greater than those measured with HEEF SN/1 at -10°C, and there should be no variation of the geometric factors with temperature.

5.2 Possible Additional Front SSD Shielding and Mass Reduction

HEEF SN/1 in CRRES had measured SSDF count rates of up to 1.5 MHz under the worst case electron flux conditions. This is the fully corrected input count rate, and under these conditions the compression counter for the S1F count overflowed about 4 times during one accumulation period of 0.512 s. Analysis of these data require careful tracking of the S1F telemetry count to ensure that the overflows are handled correctly (each overflow adds 32768 counts to the actual telemetry count). The source of the high SSDF count rate are the lower energy electrons >0.2 MeV, for which SSDF has a large geometric factor of 0.160 cm^2 sr. SSDB and the BGO scintillator have a geometric factor of about 0.012 cm^2 sr, with electron energy thresholds of >0.5 MeV (SSDB) and >0.75 MeV (BGO), so they have much lower count rates.

The reduction of the SSDF count rate requires the addition of a longer telescope for the first collimator in the set of three that define the HEEF acceptance FOV for electrons (the three tungsten collimators shown in Figure 2). Since electrons scatter significantly in the SSDs and the entrance Be foil, all three collimators affect the geometric factor. By moving the outermost collimator from the present separation of 0.5 inch out to 4.6 inch, and maintaining the collimator opening edge at an angle of 5° to the FOV center, it is possible to reduce the SSDF geometric factor to 0.034 cm^2 sr, about a factor of 4.7 reduction. This would reduce the SSDF geometric factor enough to avoid S1F overflows, and by reducing the maximum input count rate to about 300 kHz the deadtime corrections would become much less.

This change would reduce the SSDB and BGO geometric factors to about 0.007 cm^2 sr, about a factor of 1.7 reduction, so the effective electron geometric factor would be reduced slightly. However, combined with the timing pulse changes of Section 5.1, the modified HEEF would still have more than a factor of 10 count rate increase over the bulk of the CRRES data, and without the large deadtime corrections. Since electrons scatter so much the actual

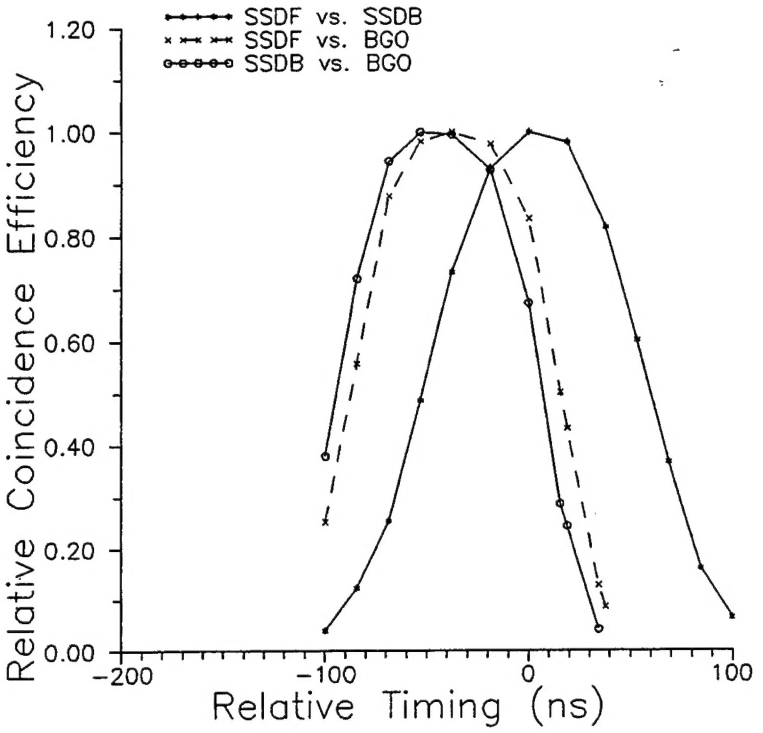

Figure 30. HEEF SN/1 Coincidence Timing Data.

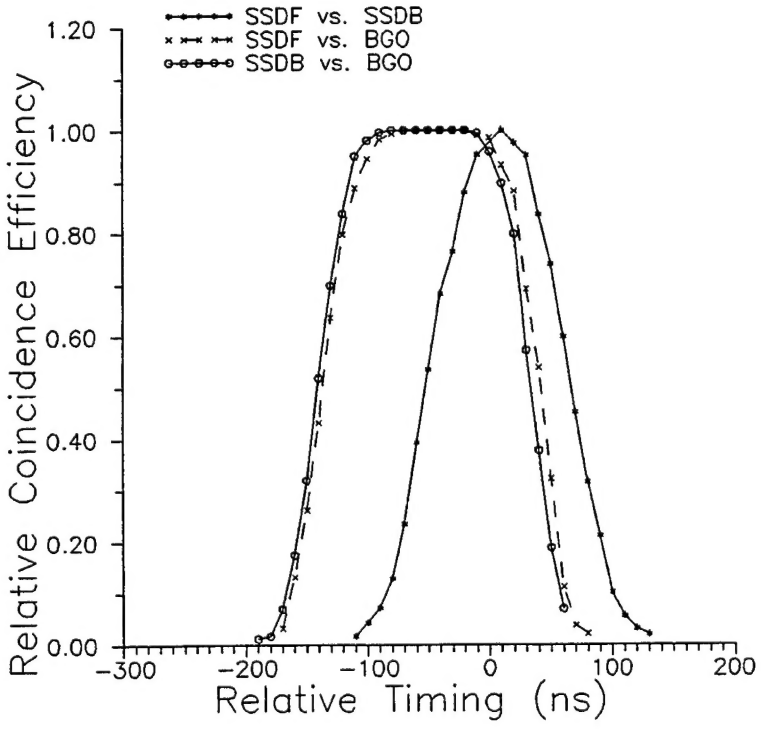

Figure 31. Modified HEEF SN/2 Coincidence Timing Data.

geometric factor change is likely to be slightly different, and the modified HEEF should be calibrated with electron beams (preferably at the MIT Van de Graaff, which has proved quite suitable).

Some additional reduction in the SSDF count rate can be made by interchanging the SSDF and SSDB detector sizes, putting the smaller detector at the FOV entrance. This would reduce the (smaller) SSDF count rate by another factor of 2, for a maximum input count rate of about 150 kHz. This change would require the interchange of the second and third collimators, but is readily accomplished with a minimum of complications. The increase in the area of SSDB would allow slightly more of the very highest energy electrons near the edge of the FOV to escape from the BGO crystal sides, but this is a small part of the total geometric factor and should not be significant.

The range of 10 MeV electrons in aluminum is 0.85 inch, while the tungsten collimators are 0.2 inch thick. Replacing the tungsten collimators with aluminum would thus require either thicker collimator edges, or the use of an inner edge of tungsten. If the collimators are replaced directly with aluminum the primary geometric factors would still be valid, but the higher energy electrons would be degraded in energy when passing through only one of the collimators, and thus produce a lower energy response. This is not likely to be a problem for steeply falling spectra (E^{-6} or so), since the contamination of low energy electrons by high energy electrons will not be a significant fraction.

Replacing all of the tungsten in the HEEF sensor with aluminum would reduce the mass from 20.8 lb to about 10.5 lb. Most of the reduction comes from the shield around the scintillators, and this has no effect on the FOV shielding. If the only the scintillator tungsten shield is replaced with aluminum, then the mass reduction would be about 7 lbs. Adding a front collimator extension would add about 0.4 lb, so the sensor mass could definitely be reduced to 14.2 lb. This change should not cause any significant degradation in the response to electrons, nor should it significantly increase the background count rate from high energy protons. Mass reductions of the HEEF sensor is definitely possible.

6. Summary and Conclusions

The AFGL-701-2/Dosimeter and AFGL-701-4/HEEF on CRRES have provided over 1000 orbits of radiation belt particle data, over a period of more than one year. The dosimeter has worked properly for the entire time period, while HEEF has provided electron flux data with a reduced geometric factor because of operation at low temperature. The corrected electron flux data from HEEF are in reasonable agreement with the dosimeter electron channel count rates.

References

1. P. R. Morel, F. Hanser, B. Sellers, J. L. Hunerwadel, R. Cohen, B. D. Kane and B. K. Dichter, "Fabricate, Calibrate and Test a Dosimeter for Integration into the CRRES Satellite", GL-TR-89-0152 (April 1989), ADA213812.

2. B. K. Dichter and F. A. Hanser, "Development and Use of Data Analysis Procedures for the CRRES Payloads AFGL-701-2/Dosimeter and AFGL-701-4/Fluxmeter and Application of the Data Analysis Results to Improve the Static and Dynamic Models of the Earth's Radiation Belts", PL-TR-92-2066 (March 1992), ADA253287.

3. B. K. Dichter and F. A. Hanser, "Development and Use of Data Analysis Procedures for the CRRES Payloads AFGL-701-2/Dosimeter and AFGL-701-4/Fluxmeter and Application of the Data Analysis Results to Improve the Static and Dynamic Models of the Earth's Radiation Belts", GL-TR-89-0284 (October 1989), ADA219479.

4. B. K. Dichter and F. A. Hanser, "Development and Use of Data Analysis Procedures for the CRRES Payloads AFGL-701-2/Dosimeter and AFGL-701-4/Fluxmeter and Application of the Data Analysis Results to Improve the Static and Dynamic Models of the Earth's Radiation Belts", PL-TR-91-2186 (July 1991), ADA241399.

5. B. K. Dichter and F. A. Hanser, "Development and Use of Data Analysis Procedures for the CRRES Payloads AFGL-701-2/Dosimeter and AFGL-701-4/Fluxmeter and Application of the Data Analysis Results to Improve the Static and Dynamic Models of the Earth's Radiation Belts", PL-TR-92-2223 (August 1992), ADA258710.

6. M. J. Berger and S. M. Seltzer, "Tables of Energy Losses and Ranges of Electrons and Positrons", NASA SP-3012 (1964).

7. M. S. Gussenhoven, E. G. Mullen, R. C. Filz, F. A. Hanser and K. A. Lynch, "Space Radiation Dosimeter SSJ* for the Block 5D/Flight 7 DMSP Satellite: Calibration and Data Presentation", AFGL-TR-86-0065 (20 March 1986), Environmental Research Papers, No. 949, ADA172178.

8. G. Auchampaugh and T. Cayton, "CRRES Dosimeter Simulations", Report LA-12511-MS, (UC-000, April 1993).

9. Quarterly Report No. 4, prepared by Panametrics, Inc. for Phillips Laboratory, Geophysics Directorate, for Contract No. F19628-93-C-0151 (PASPANA-QR-4, for the period April 23, 1994 to July 22, 1994).